Journal Pre-proofs

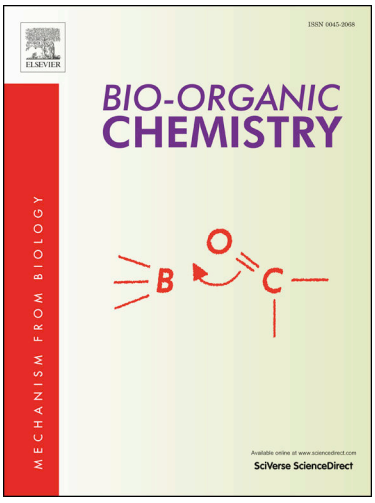

Design and synthesis of 3,5-substituted 1,2,4-oxadiazoles as catalytic inhibitors of human DNA topoisomerase IIα

Kaja Bergant Loboda, Katja Valjavec, Martina Štampar, Gerhard Wolber, Bojana Žegura, Metka Filipič, Marija Sollner Dolenc, Andrej Perdih

PII: S0045-2068(20)30121-8
DOI: https://doi.org/10.1016/j.bioorg.2020.103828
Reference: YBIOO 103828

To appear in: *Bioorganic Chemistry*

Received Date: 16 January 2020
Revised Date: 20 March 2020
Accepted Date: 5 April 2020

Please cite this article as: K. Bergant Loboda, K. Valjavec, M. Štampar, G. Wolber, B. Žegura, M. Filipič, M. Sollner Dolenc, A. Perdih, Design and synthesis of 3,5-substituted 1,2,4-oxadiazoles as catalytic inhibitors of human DNA topoisomerase IIα, *Bioorganic Chemistry* (2020), doi: https://doi.org/10.1016/j.bioorg.2020.103828

Design and synthesis of 3,5-substituted 1,2,4-oxadiazoles as catalytic inhibitors of human DNA topoisomerase IIα

Kaja Bergant Loboda[†1,2], Katja Valjavec[†1], Martina Štampar[3], Gerhard Wolber[4], Bojana Žegura[3], Metka Filipič[3], Marija Sollner Dolenc,[2] and Andrej Perdih[1]*

[1]*National Institute of Chemistry, Hajdrihova 19, SI 1000 Ljubljana, Slovenia*

[2] *University of Ljubljana, Faculty of Pharmacy, Aškerčeva 7, SI 1000 Ljubljana, Slovenia*

[3]*National Institute of Biology, Department of Genetic Toxicology and Cancer Biology, Večna pot 111, 1000 Ljubljana, Slovenia*

[4]*Institute of Pharmacy, Freie Universität Berlin, Königin Luise-Strasse 2+4, 14195 Berlin, Germany*

KEYWORDS: human DNA topoisomerase IIα, catalytic inhibitors, drug design, oxadiazoles, anticancer agents

[†] *These two authors contributed equally to this work.*

*Corresponding author:
Andrej Perdih
National Institute of Chemistry
Hajdrihova 19, SI-1001 Ljubljana, Slovenia
Tel.: +386-1-4760-376
e-mail: andrej.perdih@ki.si

GRAPHICAL ABSTRACT

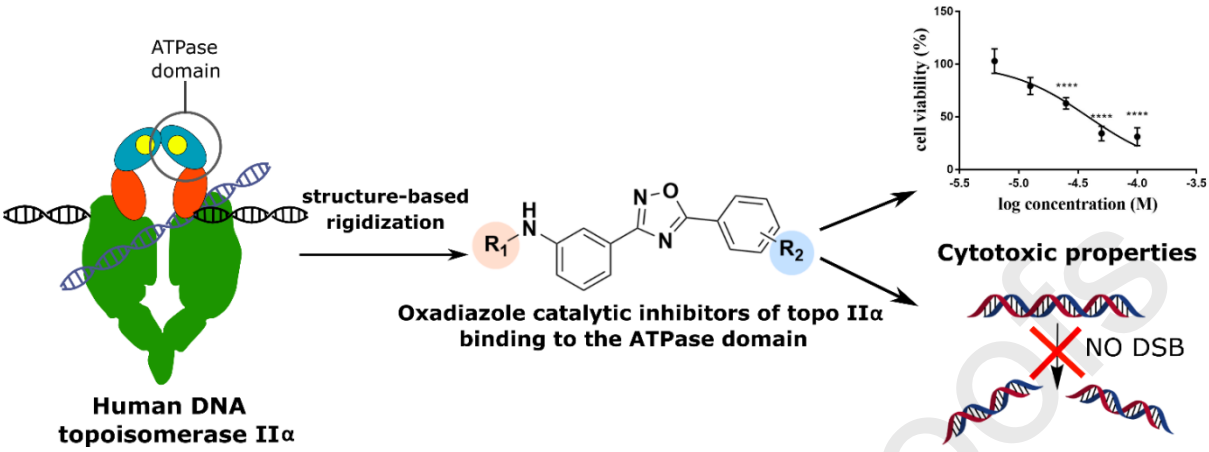

ABSTRACT

Cancer constitutes a group of diseases linked to abnormal cell growth that can potentially spread to other parts of the body and is one of the most common causes of death. The molecular motors - DNA topoisomerases - that enable topological changes of the DNA molecule are one of the most established targets of cancer therapies. Due to known limitations of established topo II poisons such as cardiotoxicity, induction of secondary malignancies and recognized cancer cell resistance, an emerging group of catalytic topo II inhibitors attempts to circumvent these challenges. Currently, this approach comprises several subgroups of mechanistically diverse inhibitors, one of which are compounds that act by binding to their ATPase domain.

In this study we have designed, synthesized and characterized a new series of 3,5-substituted 1,2,4-oxadiazoles that act as catalytic inhibitors of human topo IIα. The introduction of the substituted rigid substitutions on the oxadiazole backbone was intended to enhance the interactions with the ATP binding site. In the inhibition assays selected compounds revealed a new class of catalytic inhibitors targeting this molecular motor and showed binding to the isolated topo IIα ATPase domain. The predicted inhibitor binding geometries were evaluated in molecular dynamics simulations and subsequently dynophore models were derived, which provided a deeper insight into molecular recognition with its macromolecular target. Selected compounds also displayed *in vitro* cytotoxicity on the investigated MCF-7 cancer cell line and did not induce double-strand breaks (DSB), thus displaying a mechanism of action diverse from the topo II poisons also on the cellular level. The substituted oxadiazoles thus comprise a chemical class of interesting compounds that are synthetically fully amenable for further optimization to anticancer drugs.

1. INTRODUCTION

Cancer is one of the most prevalent diseases, and recent predictions based on 2010-2012 data suggest that about 39.6% of men and women will be diagnosed with cancer at some point in their lives [1]. In 2018, 9.6 million deaths were recorded based on the WHO data, corresponding to about 1 in 6 deaths. As a complex multifunctional disease, the true origins of cancer are still not fully understood. In their seminal papers Hanahan and Weinberg described the biological capabilities acquired during the multi-step development of human tumors, known as the "hallmarks of cancer" [2, 3], one of which is uncontrolled cell division.

DNA topoisomerases are the DNA topology altering enzymes belonging to the group of molecular motors. Some of its members require the energy of the ATP molecules to direct the DNA molecular motion [4, 5]. As their primary function they regulate the DNA topology by disentangling chromosome segments via their ability to cleave, manipulate, and religate DNA strands [5].

Topoisomerases are divided into two large groups: Type I topoisomerases which can catalyze topological changes within one DNA molecule and Type II topoisomerases which can catalyze such changes affecting two segments of the DNA molecule. Type II refers here to the fact that these enzymes can cleave both strands of one double-stranded DNA segment, in contrast to Type I, which cleaves only one strand within a double-stranded DNA molecule [4, 6]. In addition, Type II topoisomerases for its successful catalytic activity require the presence of Mg^{2+} ions along with the mentioned ATP molecules. [7].

The catalytic cycle of human topoisomerase IIα is a complex, multistep process in which ATP hydrolysis, in conjunction with the controlled association and dissociation of multiple subunits, leads to the passage of one DNA chain through another by means of cleavage [8, 9]. Despite intensive research a lot of mechanistic steps remain unclear, especially with the conformational changes associated with the passage of the T-segment via a cleaved G-segment of the DNA [4, 10].

Human DNA topoisomerase II α is a well-known target used in anticancer therapy. Inhibitors of human topo IIα are in the literature divided into two large groups: topo II poisons and catalytic inhibitors [11, 12]. The more established group, topo II poisons, act by stabilizing the short-lived covalent complex formed between the topo II enzyme and the T-segment of the DNA. This in turn leads to permanent breaks in the cell DNA, resulting in chromosome translocations and finally apoptosis. The examples of topoisomerase poisons that are already included in standard clinical practice are well-known molecules such as etoposide [13] and doxorubicin [14]. The development of new topo II poisons that are currently undergoing clinical trials include various and diverse molecules among them compounds such as Voreloxin, C-1311 and R(+)XK469 [15].

Alternatively, a new emerging group of catalytic topo II inhibitors was designed to avoid the well-known side effects of topo II poisons such as cardiotoxicity and induction of secondary malignancies [14, 16]. In addition, the increased resistance to topo II cancer therapies is also a further challenge for successful therapy. Here, diverse and mechanistically different-acting groups of compounds aim to inhibit the topo II catalytic cycle without the stabilization of the covalent cleavage complex [12]. The groups can act via an inhibition of binding between the DNA and topo II (e.g. aclarubicin and suramine) [17, 18], inhibition of the DNA cleavage (e.g. merbarone) [19], inhibition of the ATP hydrolysis and capturing of topo II in a closed clamp (e.g. ICRF group of compounds) [20, 21] and finally, via inhibition of binding of the ATP molecule in its binding site (e.g. gambogic acid) [22-26].

Previously, our research has been directed to explore the potential of the last-mentioned approach to catalytic topo II inhibition. In our efforts we have characterized several classes of catalytic inhibitors, that target the ATP binding site including triazin-2(1*H*)-ones [27, 28], 1,3,5-triazines [29], 1*H*-pyrazolo[3,4]pyrimidines [30], 9*H*-purines [30] and 1*H*-indazoles [31]. In the scope of our broader investigation of the type II topoisomerase were also exploring the

inhibition of the bacterial type II counterpart, the bacterial DNA gyrase, focusing on its ATP binding site. Among many of our research activities here we also identified a series of substituted oxadiazoles that have been designed and synthesized as potential DNA gyrase inhibitors [32].

In this study we used a structure-based approach to design derivatives of 3,5-substituted 1,2,4-oxadiazoles that could act as catalytic inhibitors of human topo IIα molecular motor. The schematic outline of the research process is shown in Scheme 1. The introduction of the substituted rigid moieties into the initially available flexible, non-active oxadiazoles served to enhance the interactions with the targeted human topo IIα ATP binding site. After initial SAR assessment of the two main substituents attached to the core scaffold, a second series of 3,5-substituted 1,2,4-oxadiazoles was synthesized. We then included a small series of reversely substituted commercially available 3,5-substituted 1,2,4-oxadiazoles in the inhibitor screening process to broaden the SAR of our initial synthesized series. We evaluated the inhibition of topo IIα with a high-throughput screening (HTS) relaxation assay, and for selected active compounds the mechanism of topo IIα inhibition was further investigated with a cleavage assay and SPR binding experiments. Predicted inhibitor binding was evaluated in a molecular dynamics (MD) simulation, and subsequently a dynophore model - dynamic 3D pharmacophore - was derived to gain deeper insight into the molecular recognition of this class of compounds with their macromolecular target. At the cellular level, MTS cytotoxicity measurements and analysis of the induction of the DNA double-strand breaks (DSB) by γ-H2AX assay were performed on the MCF-7 breast cancer cell line to evaluate their genotoxic potential.

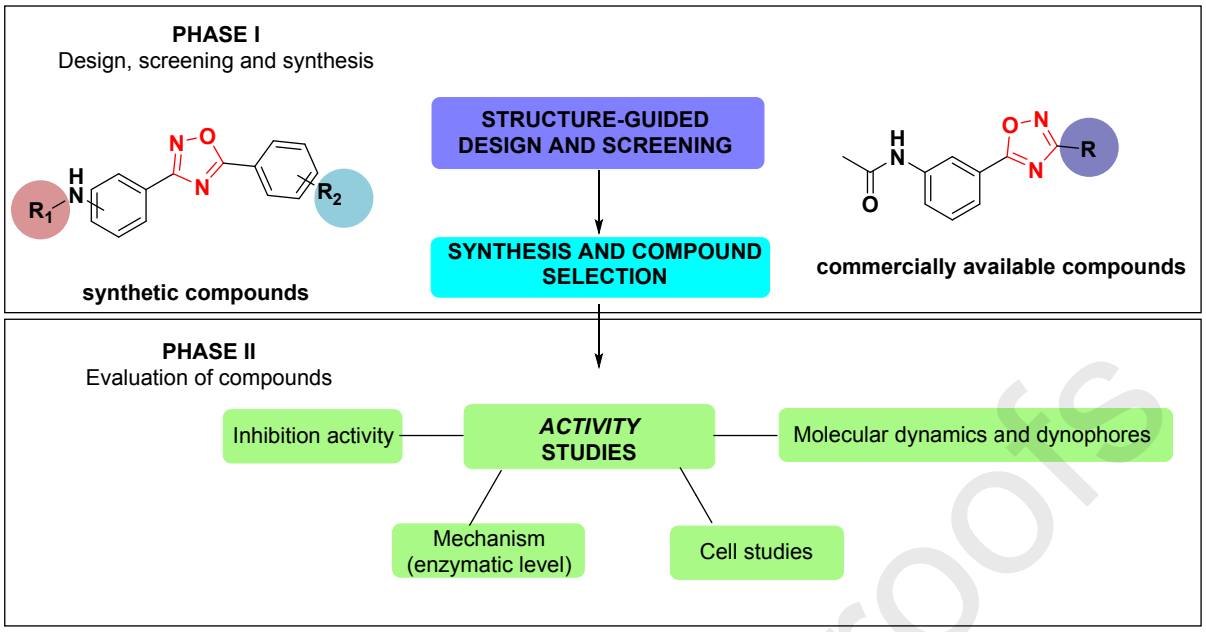

Scheme 1. Schematic outline of the workflow used in the identification of the 3,5-substituted 1,2,4-oxadiazoles as catalytic inhibitors of the human DNA topoisomerase IIα.

2. RESULTS AND DISCUSSION

2.1. Design of 3,5-substituted 1,2,4-oxadiazoles

Our research started with a small subset of the available flexible 3,5-substituted-1,2,4-oxadiazole compounds A-D, which were previously designed in our research activities as potential inhibitors of the bacterial type II topoisomerase - DNA gyrase [data not shown]. Unfortunately, when the topo IIα HTS relaxation assay was performed, these compounds were all classified as inactive (see Supplementary material, Table S1). Not discouraged by this result, we have decided to try to optimize their structure in order to achieve a better fit into the ATP binding site of the human topo IIα.

In a first step we docked the oxadiazole compound **A** into the ATP binding site of the human topo IIα ATPase domain (PDB: 1ZXM) using GOLD program [33]. Subsequently, we visualized the results with LigandScout [34], which enabled us to generate the 3D structure-based pharmacophores thus pinpointing the key intermolecular interactions (Figure 1). In this process we observed that the acetylated amino group on one phenyl ring attached to the oxadiazole of compound **A** forms an interaction with Asn120 in the human topo IIα ATP binding site, which is the anchoring residue of the native ATP ligand adenine moiety. In addition, the carboxylic group attached on the flexible aliphatic chain points to the residues normally occupied by the interactions between the phosphate groups and their binding site, such as Lys168.

Although the compounds **A-D** were all rendered inactive, we speculated that the aniline-substituted 1,2,4-oxadiazole scaffold, after appropriate modification, might allow favorable interactions with the ATP binding site to such an extent that inhibition of the target enzyme could be achieved. Therefore, in the first design step, we replaced the flexible chain substituent attached to the oxadiazole core with a phenyl ring substituent also containing different functional groups. In this way, we aimed to increase the rigidity of the compounds and introduce

such substituents/functional groups that would allow interactions with the "triphosphate" part of the ATP binding site (Figure 1). The first compound of the 3,5-substituted 1,2,4-oxadiazoles designed in this way was compound **3a**, which contains the carboxyl group in its ester form on the phenyl ring.

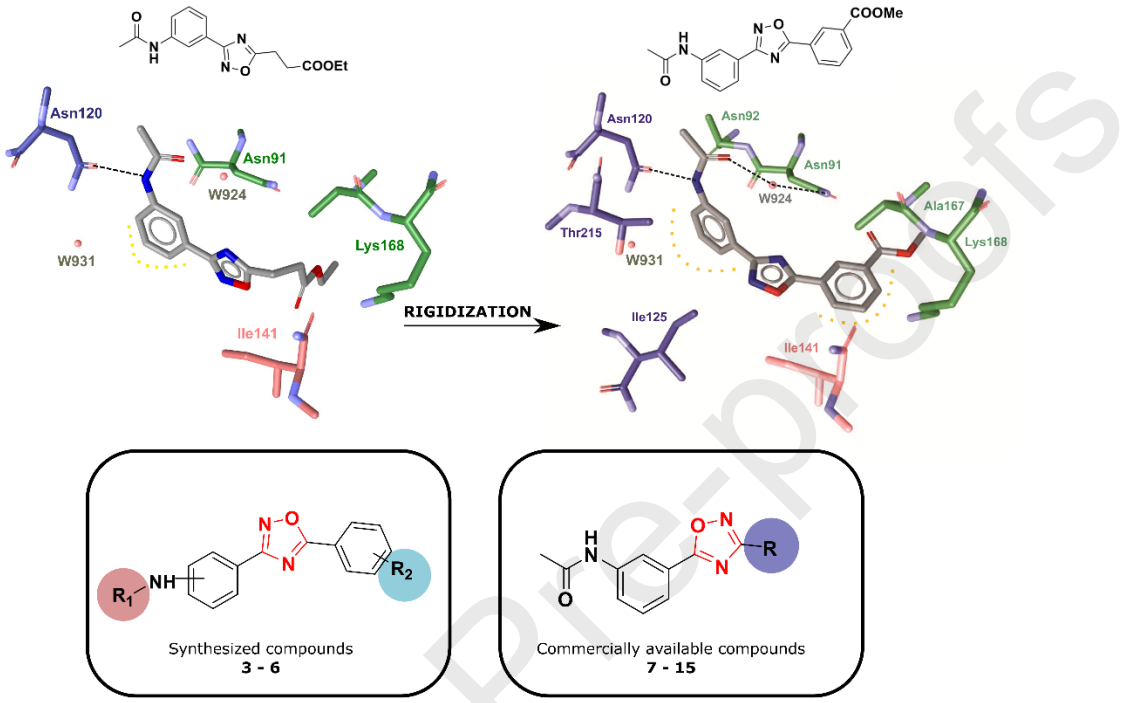

Figure 1. Predicted binding modes of the inactive oxadiazole compound **A** and the designed rigid 3,5-subtituted 1,2,4-oxadiazole **3a** in the topo IIα ATP binding site (PDB:1ZXM). Bellow: General structures of the targeted synthesized 3,5-substituted 1,2,4-oxadiazoles **3-6** (left) selected commercially available substituted 3,5-substituted 1,2,4-oxadiazoles **7-15** (right).

To investigate how such oxadiazole compounds can accommodate the ATP binding site, we again performed the docking calculations of the designed oxadiazole **3a** (Figure 1). When analyzing the obtained binding models, we again observed that the residue Asn120 forms an H-bond interaction with the amido group on the 3-phenyl ring, which is bound to the 1,2,4-oxadiazole scaffold. We also detected the presence of a water-mediated interaction between the Asn91 residue and the X-ray detected crystal water W924, which was included in the definition

of the binding site, as in our previous studies, [23, 27, 30], under the assumption that it could form an important interaction. Hydrophobic interactions were formed between the two phenyl substituents and the amino acids Ile125, Ile141, Phe142 and Ala167. The subsequently generated 3D structure-based pharmacophore detected further favorable interactions with the amino acids Lys168, Arg162 and Thr165 in the "ribose sugar" part and in the "triphosphate" part of the ATP binding pocket. Additional comparison of the docked binding mode of active compound **3a** and a non-hydrolysable AMP-PNP ligand in the human DNA topoisomerase IIα ATP binding site (PDB:1ZXM) is shown in Supplementary material, Figure S2.

In the original oxadiazole series **A-D**, the acylated amino group substituent was present either at meta or para position and its carboxylic group was present in both the free acid and ester forms. To explore this chemical space in our new series, we decided to vary the position of the carboxyl moiety attached to the phenyl ring as well as the position of the acylated amino group. In design phase 1 we synthesized the first 9 target compounds **3a**, **3b**, **4a**, **4b**, **5a**, **5b**, **5k**, **6a** and **6b** (Table 1). After identifying the best position of the substituents in phase 2, further 16 compounds **3-5** (Table 1 and 2) were synthesized to broaden the SAR of this chemical class. In this step we also investigated the influence of the acyl substitution of the amino group present on the first phenyl ring on topo IIα function.

In an attempt to broaden the SAR data, we also looked for commercially available 3,5-substituted 1,2,4-oxadiazoles with a similar interaction pattern (Table S2). Since only oxadiazoles that showed a reverse phenyl substitution pattern compared to the main oxazole scaffold were available, we decided to include them in the screening process in the hope of possibly identifying further active compounds along with obtaining new SAR data. As a result, 9 compounds **7-15** were selected and tested experimentally (Table 3). Proposed docking binding mode of the active, commercially available compound **7** in human DNA topoisomerase IIα ATP binding site (PDB:1ZXM) is shown in Supplementary material, Figure S3.

2.2. Synthesis of the 3,5-substituted 1,2,4-oxadiazoles

Designed 3,5-substituted 1,2,4-oxadiazoles **3-6** were synthesized using a synthetic route presented in Scheme 2. From the starting compounds 3-aminobenzonitrile (**Ia**) and 4-aminobenzonitrile (**Ib**), the corresponding acetamide (**IIa** or **IIb**) was synthesized by the procedure already tested [35]. In this way, the amine group was protected from further reactions, since it exhibits nucleophilic properties, and at the same time the acetamide group is also important for interaction with the topoisomerase IIα binding site.

Synthesis of compound **Ia** proceeded rapidly in fairly high yields (about 90%), which were similar to that of compound **Ib**. It was synthesized by the same procedure as compound **Ia**, but the reaction took longer (48 hours), unlike compound **Ia**, where the reaction was completed in half an hour, which is due to the favorable electronic effects of the ciano group. A further step in the synthesis of the final compounds was the conversion of the cyano group to amidoxime (Compounds **IIIa**, **IIIb**), which was performed according to a standard procedure with hydroxylammonium chloride in ethanol [36]. It is the nucleophilic addition of the amine group of hydroxylamine to the electrophilic carbon of the cyano group on the benzene ring of compounds **IIa** and **IIb**, which leads to the formation of amidoxime.

The third step in the synthesis of the final compounds was the O-acylation of the amidoximes (Supplementary material, **Table S3**) that we had synthesized in the previous step. The acid chlorides or the corresponding acids (for compounds **3c**, **3j**, **5j**), previously activated for nucleophilic substitution with the hydroxyl group of amidoxime, were selected as the acylating agents (Supplementary material, **Table S4**). Most often, activation of the selected acids in mixed anhydride with ethyl chloroformate was used.

The preparation of O-acylated amidoxime was carried out in both ways with appropriate efficiencies (from 29% to 97%) but was slightly lower in the case of acid activation, since the activation was carried out *in situ.* There are several possible synthetic routes for the synthesis

of 3,5-disubstituted 1,2,4-oxadiazole rings: 1,3-dipolar cycloaddition of nitriles with nitrile oxides, condensation of amidoxime with carboxylic acids and their derivatives, oxidation of aldoxime and N-substituted amidoxime [37]. In our case, we chose the cyclization of O-acylamidoxime, which we were able to isolate in the previous stage of synthesis. Intramolecular condensation preceded, first a nucleophilic addition between the amine group and the acyl carbonyl carbon atom, followed by a water removal. The planned 3,5-disubstituted 1,2,4-oxadiazoles were synthesized in anhydrous toluene at boiling point, and the reaction mixture was purged with argon to provide anhydrous conditions. The reactions were carried out for several days, but in this way, we obtained very pure products which, after isolation, had to be further purified by column chromatography in only a few cases. For the preparation of compounds **5a**, **5b**, **6a**, **6b**, basic hydrolysis (saponification of the ester) was performed, and the acetamide groups of **5c-k** compounds were removed by acid hydrolysis. In most cases, the compounds were synthesized from the basic building blocks in 3 or 4 steps, and the synthesis pathways for these compounds are appropriate.

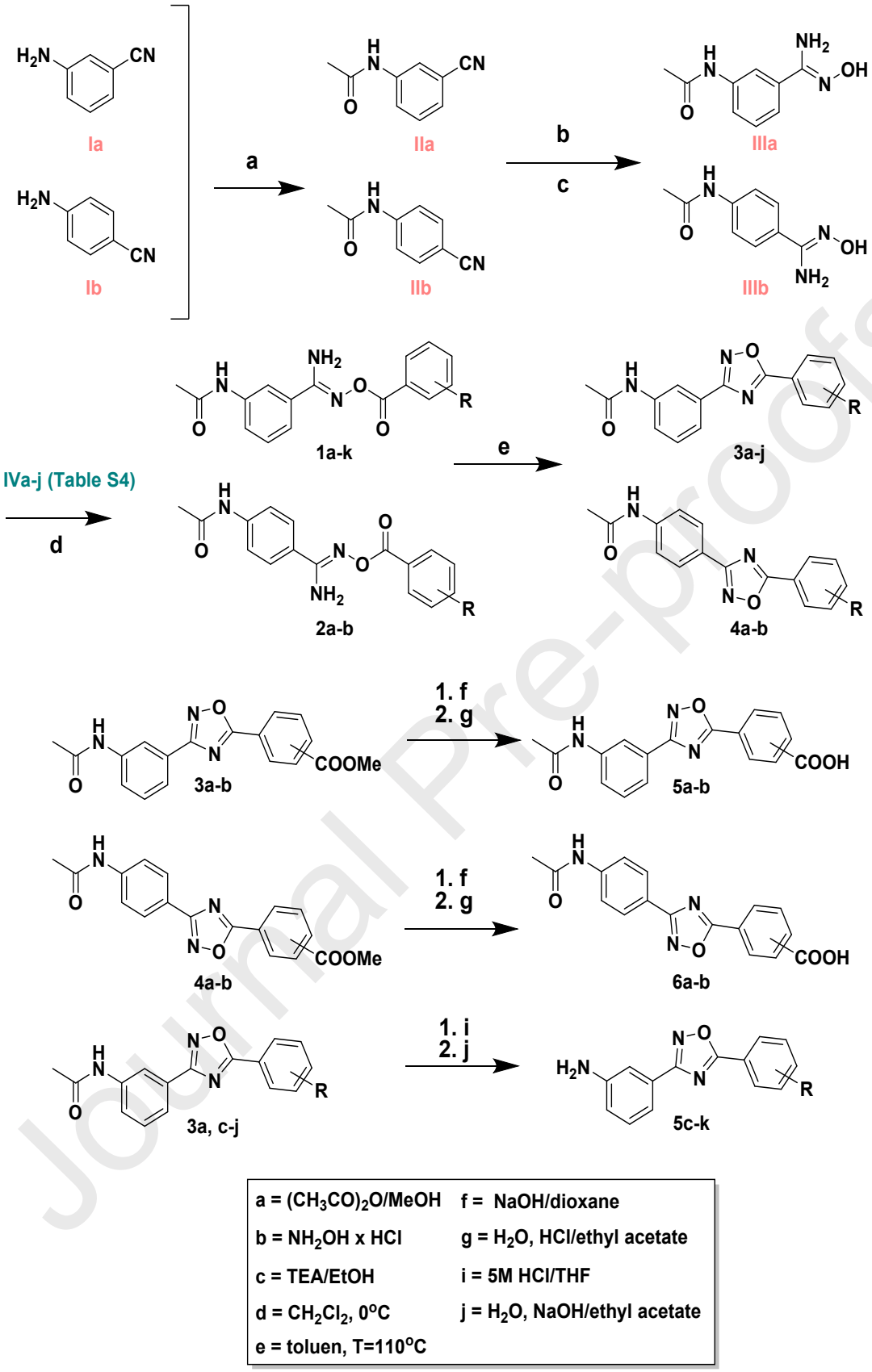

Scheme 2. General synthetic scheme for the synthesis of the targeted 3,5-substituted 1,2,4-oxadiazoles **3-6**.

2.3. Human topo IIα HTS inhibition assay and initial SAR of the synthesized and commercially available 3,5-substituted 1,2,4-oxadiazoles

The synthesized and commercially available compounds **3**-**15** were experimentally assayed if they inhibit catalytic activity of the human topo IIα using a standard topo II high-throughput screening (HTS) relaxation assay [38]. To validate the assay, etoposide was used as control compound, for which we experimentally determined the value of 41.6 μM which adequately compares to the 60.3 μM value, reported in the literature [39]. Results of assay of the two synthesized series marked by compounds **3**-**6** are available in Table 1 and Table 2. It should also be pointed out, that all synthesized final compounds **3**-**6** as well commercially acquired oxadiazoles **7**-**15** were found to possess drug-like properties characterized by the favorable predicted logP [40] values lower than 5 and topological Polar Surface Area (tPSA) [41] lower than 120.

After performing the assay of the initial design phase 1 series was gratifying to observe that some synthesized compounds of the first series compounds showed to be inhibitors of the human topo IIα. To the best of our knowledge this represents the first compounds of the 3,5-substituted 1,2,4-oxadiazole that act on this human type II topoisomerase. For the most active compound **3a** an average IC_{50} value of 147.7 ± 10.6 μM was determined which is in comparable range, although still about 2.5-fold higher than the etoposide reference drug. The initial SAR of the assay also pointed out that meta substitution of both phenyl rings attached to the core 1,2,4-oxadiazole is the most optimal substitution position for the inhibition activity.

Table 1. Structures of the synthesized 3,5-substituted 1,2,4-oxadiazoles **3**-**6** and their IC_{50} values determined in the topo IIα HTS screening relaxation assay (design phase 1).

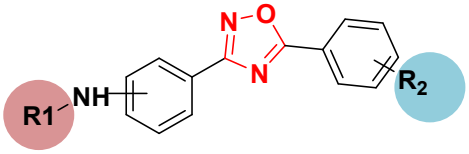

Compound	R1	R2	IC_{50} (μM)
3a	3-($COCH_3$)	3-(COOMe)	147.7
5a	3-($COCH_3$)	3-(COOH)	657.8
5k	3-H	3-(COOMe)	>1000
3b	3-($COCH_3$)	4-(COOMe)	>1000
5b	3-($COCH_3$)	4-(COOH)	>1000
4a	4-($COCH_3$)	3-(COOMe)	700.6
6a	4-($COCH_3$)	3-(COOH)	>1000
4b	4-($COCH_3$)	4-(COOMe)	>1000
6b	4-($COCH_3$)	4-(COOH)	>1000

In the design phase II, we kept the meta position of the amide or the appropriate free amine on of 3-phenyl ring fixed and varied the R2 substituents introduced on the 5-phenyl ring. As a result, we introduced various meta- and para- substituted phenyls that were synthetically available (Table 2). Some of the flour- and choro- derivatives were included due to substantial similarity of the docking placement of such R2 substituted phenyl ring and a corresponding substituent present in our recently reported 4,6-substituted-1,3,5-triazin-2(1*H*)-ones occupying the same position in the ATP binding site (Figure S4) [28]. Inhibitory relaxation assays identified 7 new compounds possessing minimal topo IIα inhibitory activity with compounds **3f** and **5g** possessing the most promising IC_{50} values 284.2 μM and 311.3 μM, respectively. From these results, we obtained relevant SAR information that both free amide or amine on the

meta R1 position can lead to topo II inhibition activity. The new substituents also identified some of the new R2 substituents, with compound **3f** possessing the trifluoro substituent on the 5-phenyl ring and **5g** a methoxy substituent which exhibited comparable activity to the initially synthesized compound **3a**.

Table 2. Structures and IC_{50} values of the synthesized 3,5-substituted oxadiazoles **3-5** determined in the topo IIα HTS screening relaxation assay (Design Phase 2).

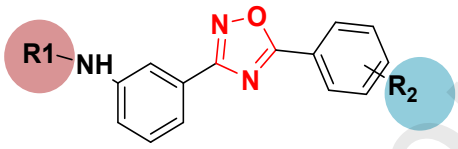

Compound	R1	R2	IC_{50} (μM)
3c	-($COCH_3$)	3-(Cl)	461.4
5c	-H	3-(Cl)	>1000
3d	- ($COCH_3$)	4-(Cl)	>1000
5d	-H	4-(Cl)	433.6
3e	-($COCH_3$)	3-(CF_3)	657.4
5e	-H	3-(CF_3)	>1000
3f	- ($COCH_3$)	4-(CF_3)	284.2
5f	-H	4-(CF_3)	>1000
3g	-($COCH_3$)	-3(OMe)	>1000
5g	-H	-3(OMe)	311.3
3h	-($COCH_3$)	-4(OMe)	>1000
5h	-H	-4(OMe)	585.1
3i	-($COCH_3$)	-4(NO_2)	>1000

5i	-H	-4(NO_2)	>1000
3j	-($COCH_3$)	-3F, -5(CF_3)	523.9
5j	-H	-3F, -5(CF_3)	>1000

To further investigate the chemically space of this compound class we decided to select and assay also a small subset of commercially available 3,5-substituted 1,2,4-oxadiazoles **7-15** with different "reverse" substitutions of the phenyl rings (Table 3). We decided for this search also because the position of the nitrogen functionality of the 3-phenyl ring was not available in the pool of commercially available molecules. In this manner, we now varied the functional groups on the phenyl at the position 3 of the oxadiazole scaffold and fixed the acetylated amino group on the 5-phenyl ring. We made several searches using the e-molecules search engine and after molecular docking analysis of the approximately 100 available compounds acquired 9 new oxadiazoles for inhibition assay.

From the selection, compounds, **10**, **11** and **12** showed the IC_{50} inhibitory activities of 226.1 μM, 165.9 μM and 162.7 μM, respectively, these being of comparable potency to the Phase 1 synthesized compound **3a.** By determining the inhibition activity of these compounds, we also showed that reverse 3,5-phenyl substitution pattern of the core oxadiazole ring, with the acetylated amino group being fixed to the 5-phenyl ring also enables the inhibition activity. Besides the already investigated methoxy substituent (**7**) more complex piperidine (**10,11**) and morpholine moieties (**12**), attached to phenyl ring via either an amido or sulfonyl group were rendered as favorable for the topo IIα inhibition activity broadening the compounds SAR.

Table 3. Determined IC_{50} values of the commercially available 3,5-substituted 1,2,4-oxadiazoles **7-15** in the topo IIα HTS screening relaxation assay.

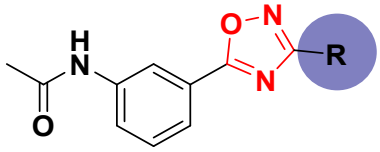

Compound number	R	IC_{50} (μM)
7	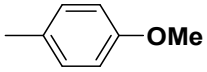	507.7
8	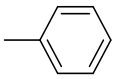	455.3
9	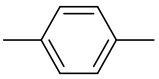	>1000
10	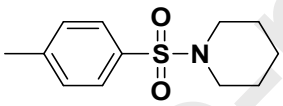	226.1
11	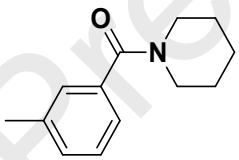	165.9
12	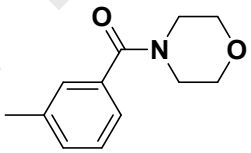	162.7
13	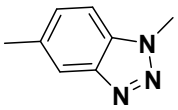	>1000
14	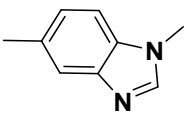	>1000
15	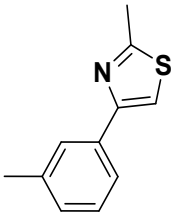	>1000

To investigate and compare reversely substituted oxadiazoles, with our synthesized oxadiazoles, docking poses and 3D structure-based pharmacophores of active compounds **10** and **11** (Figure 2) were calculated. Amido group placed on the 5-phenyl ring of the 1,2,4-oxadiazoles formed a hydrogen bond with Asn120 in the ATP pocket. Such compound placement can be rendered fully comparable with what we observed previously when the nitrogen functionality was placed on the 3-phenyl ring. Standard hydrophobic interactions formed by both phenyl groups and amino acids Ile125, Ile141, Phe142 and Ala167 appear to contribute important intermolecular interactions in the derived binding model. The docking modes also detected interactions between the amido (**11**) or sulfonyl (**12**) group oxygens and the amino acids Lys168, Arg162 and Thr165 in the "ribose-sugar" part and" triphosphate" part of targeted ATP binding pocket.

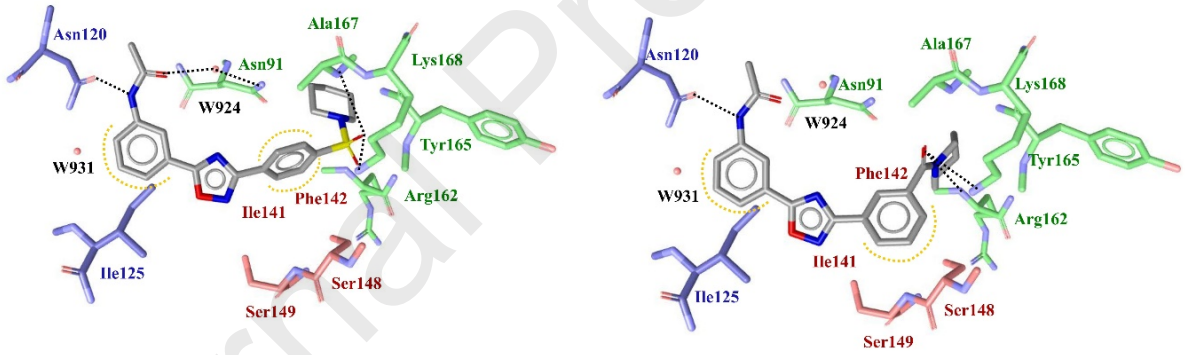

Figure 2. Predicted binding modes and 3D structure-based pharmacophores of the active commercially available reversely substituted oxadiazoles **10** and **11**.

2.4. Investigation of the topo IIα inhibition mechanism

After these initial results provided by the HTS topo IIα relaxation assay, we further investigated the inhibitory mechanism of the 3,5-substituted 1,2,4-oxadiazoles in more detail. This is a vital important step in characterizing the topo IIα inhibitors, due to the complexity of the topo IIα catalytic cycle [42].

2.4.1 3,5-substituted 1,2,4-oxadiazoles act as catalytic inhibitors of human DNA topoisomerase IIα

To investigate the mechanism of inhibition, first a topo IIα-mediated cleavage assay was performed. Human topo IIα enzyme was incubated with the negatively supercoiled plasmid and four concentrations of the oxadiazole-based inhibitor **3a** along with the topo II poison drug etoposide as a reference compound. The obtained results (Figure 3) clearly displayed the poison activity of etoposide with an increase in linear DNA with increased compound. However, the same titration with the compound **3a** and did not result in significant increase of linear plasmid above that of background (DMSO alone) so they were not considered to act as topo II poisons. The cleavage assay thus confirmed that the 3,5-substituted 1,2,4-oxadiazoles are catalytic topo II inhibitors and not topo II poisons. Detailed results of the cleavage assay are available in Supplementary material, Table S6 and Figure S6.

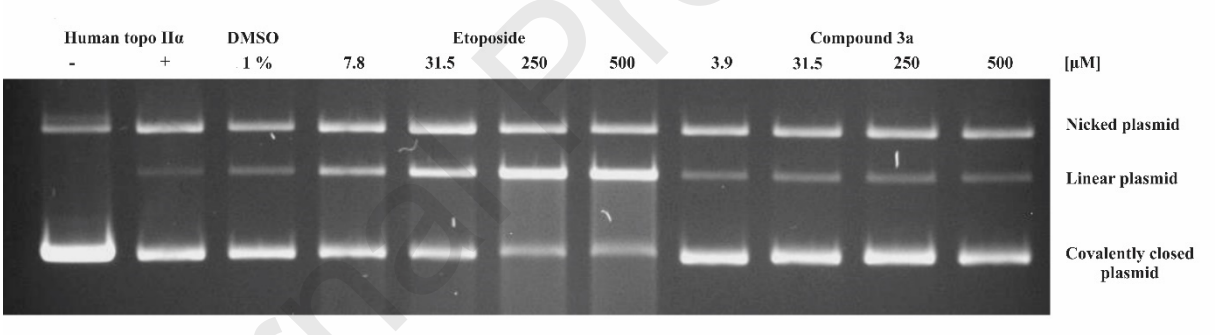

Figure 3. Results of the topo II α cleavage assay for etoposide reference and 3,5-substituted 1,2,4-oxadiazole **3a**.

2.4.2. 3,5-substituted 1,2,4-oxadiazoles bind to the isolated human topo IIα ATPase domain

The cleavage assays confirmed that compounds do not act as topo II poisons. Thus, we subsequently investigated if the inhibitory activity of compound **3a** was associated with their binding to the human topo IIα ATPase domain using surface plasmon resonance (SPR) experiments. In this binding experiment the truncated ATPase domain of human topo IIα was

immobilized on the CM5 chip and real-time sensorgrams were recorded and analyzed using Biacore T100 Evaluation Software and are provided in Supplementary material, Figure S7. General fitting and steady-state affinity, one-site binding, were calculated using Biacore Evaluation Software and graph showing response units as a function of the inhibitor concentration is supplied in Figure 4.

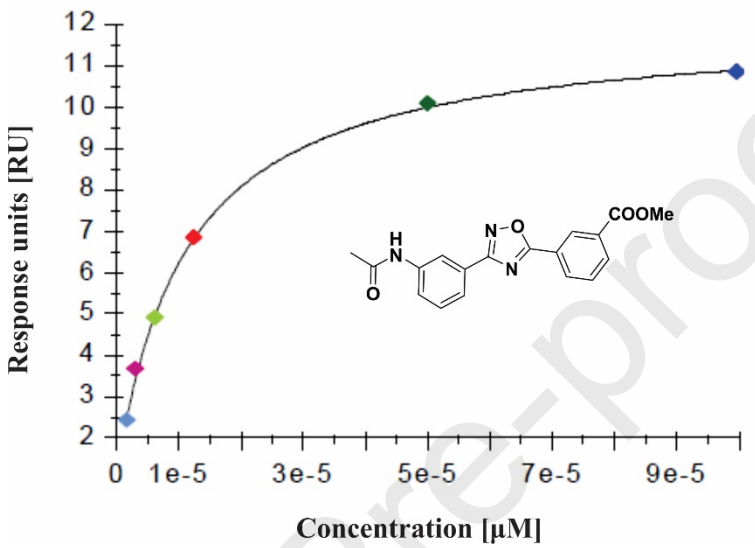

Figure 4: Results of the SPR binding experiment for compound **3a.** The binding graph is showing response units (RU) as a function of compound concentration.

Tested compound **3a** was titrated at six different concentrations in three parallel experiments, and the K_D values were determined using a steady-state affinity binding model (one-site binding). The maximal theoretical response was calculated according to the molecular masses of the human ATPase domain and compound **3a**. K_D value for the tested compound was 14.3 ± 3.4 µM. The SPR experiments confirmed that compound **3a** binds to the human topo Iiα ATPase domain where the ATP binding site is located and have consequently provided more confidence in our *in silico* models of binding, generated by molecular docking studies. The determined binding potency of our compounds to the ATPase domain also favorably compares to the reported binding of the native ATP to this domain for which the K_D value of $6.15 \pm 0.11 \times 10^{-4}$

M was determined using the same SPR methodology [43]. The binding graphs of other two parallels are represented in Supplementary material, Figure S8.

It is important to note that in the cells many existing enzymes and molecular machines similar to topo IIα exploit the energy of the ATP molecule to support various biological processes among others citric acid cycle, beta oxidation, proteins synthesis and muscle contraction. In addition, there are numerous protein kinases possessing the ATP binding site that play a vital role in the regulation of most cellular pathways [44, 45]. Thus, the issue of selectivity will be one of the aspects to explore in further optimization efforts. Interestingly, recent findings suggested that in certain cases, targeting other relevant targets (e.g. protein kinases) concurrently with topo IIα ATP inhibition might even be desired, due to resulting synergistic effects during chemotherapy [46]. All these results indicate that exciting further development of this class of topo II catalytic inhibitors is still ahead.

2.5. Analysis of the interactions of the 3,5-substituted 1,2,4-oxadiazoles in the ATP binding site using molecular dynamics (MD) and dynophore analysis

Our SPR data suggested that optimized series could bind into the ATP binding site located on the human topo IIα ATPase domain. In addition, the performed cleavage experiment confirmed that these compounds do act as topo II catalytic inhibitors. Having a static binding pose of the target-ligand complex obtained by molecular docking, we initiated molecular dynamics simulations in order to acquire insights into the flexibility [47] of the designed oxadiazole compound **3a** in its targeted ATP binding site. It is important to note that to the best of our knowledge so far, no co-crystal structure of a small molecule inhibitor bound in the human topo IIα ATP site has been reported. Using CHARMM we constructed a solvated target topo IIα-ligand system that was then equilibrated and simulated in the 20 ns MD simulation as described in the Experimental section. Animation of the observed ligand-protein conformational space is

available in the Supplementary material and a representative MD snapshot is presented in Figure 5A.

The MD trajectory was first analyzed with the RMSD parameter. Relatively low value of RMSD = 2.56 ± 0.54 Å indicates the geometric stability of the predicted docked binging pose in the human topo IIα binding site (Figure S5). Considering the calculated GOLD docking model, we first analyzed the stability of designed compound **3a** in the adenine part of the binding pocket, which, according to our previous knowledge and simulations, serves as the compound's anchor, with the amino acid Asn120 acting as the main hydrogen bond interaction (Figure 5B). Proposed interaction between the carbonyl oxygen of Asn120 and oxadiazole's ring nitrogen proved to remain fully stable during the simulation, with the average distance value of 2.90 ± 0.30 Å. Next, we analyzed the proposed interactions in the triphosphate part of the ATP binding site. Interaction with amino acid residue Ala167 remained reasonably stable at 2.90 ± 0.20 Å, regardless of relatively high flexibility of the ethylene tail of the molecule. Despite the observed interaction in the static docking pose, H-bond interaction between the compound's tail oxygen and Lys168 (d = 6.1 ± 0.8 Å) did not prove to be stable enough during MD simulation, as the residue moved away from the compound during the simulation (Figure 5A, position of Lys168).

Subsequently, we upgraded the geometrical MD analysis with a dynophore model, a powerful new method of the analysis of MD trajectories developed at the Freie Universität Berlin. Such produced dynophores aim at supplementing information provided by the classical 3D pharmacophores with the statistical and sequential information as they represent probability density clouds for each occurring intermolecular interaction during the MD simulation. In this way, the analysis of MD trajectories does not depend solely on the geometrical parameters such as intermolecular distances [48-50].

Such insight into the flexibility of the interaction pattern confirmed our observations from the geometrical analysis (Figure 5C) and provided new important insights and clues concerning the ligand molecular recognition. The hydrogen bond between the amido nitrogen and the amino acid Asn120 is present 95.0% of the time. Also, interaction between the ethylene tail oxygen and the amino acid Ala167 remains present 96.9% of the simulation time. Additionally, we observed a formation of a hydrogen bond between the oxadiazole's ring nitrogen and the amino acid Asn91, present 88.4% of the simulation time. This interaction might be complementing the water-mediated interaction of Asn91 observed earlier. It is important to mention that this interaction was not detected by the classical geometrical analysis of the MD trajectory, which verifies the valuable support of dynophore models to classical analysis of MD simulations.

Moreover, the obtained dynophore further substantiated the importance of hydrophobic interactions that could not be so easily addressed by utilizing classical parameters of geometry-based analysis (Figure 5C). Both benzene rings form hydrophobic interactions with the amino acid environment, which is present throughout the whole simulation. First benzene ring majorly interacts with amino acids Thr215 and Ile125. Second ring forms interactions with Ile14, Ala167, Phe142, and Tyr151. This type of interaction is most probably crucial for our compounds to interact with the binding site of topo IIα. In addition, the inherent characteristics of the ATP binding site imply that non-polar interactions (such as dispersion energy) importantly contribute to the stabilization of these protein-ligand complexes. To study these aspects further, application of more rigid computational techniques, such as for example Linear Interaction Energy (LIE) method developed by Åqvist and co-workers, where the electrostatic and non-polar contributions to binding free energy can be evaluated in more details would be valuable [51]. It should be also noted that ligands´ pKa values can change when compounds bind to the protein and thus influence the molecular recognition process [52, 53].

Finally, it is important also to note that MD simulation although reasonably long, still does not enable an extensive coverage of the conformational space for an unambiguous quantitative ligand stability assessment. However, it should be emphasized that in the absence of a complex human topo IIα crystal structure this approach still provides some initial clues of the ligand dynamics, especially since the SPR experiments confirmed the interaction with the ATPase domain [54].

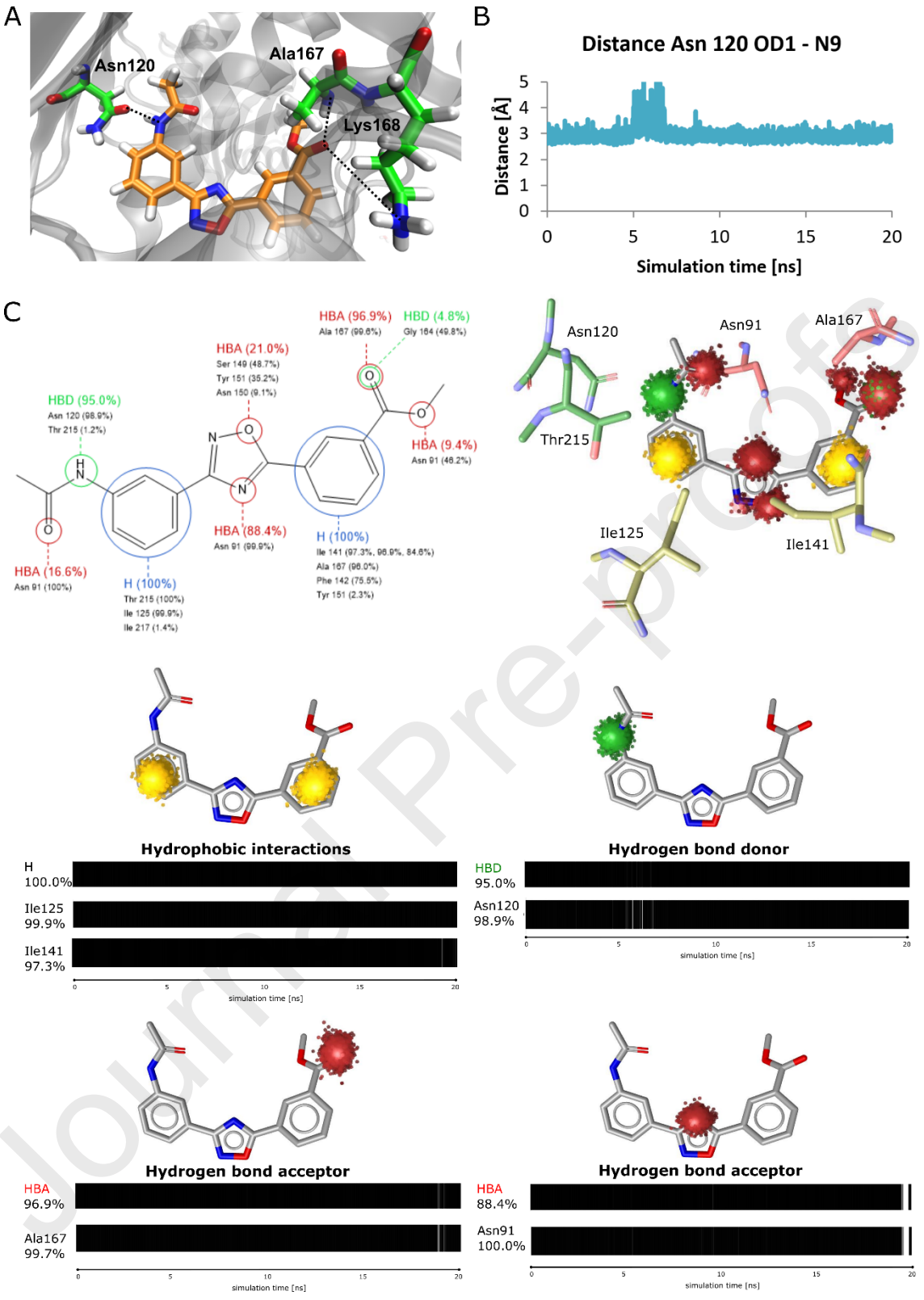

Figure 5. (**A**) Representative MD snapshot of compound **3a** in the ATP binding site of the human topo IIα. (**B**) Time-dependence graph for the distance between the OD1 atom of Asn120 and the N9 nitrogen of compound **3a** (**C**). An overview of the interaction pattern obtained with

the dynophore analysis: (Left): Calculated percentage of occurrence of a dynamic pharmacophore element on the basis of all frames broken into element-interacting amino acids pairs; (Right): Full calculated dynophore model of compound **3a** presented with pharmacophore feature types – hydrogen bond donor, HBD (green), hydrogen bond acceptors, HBA (red) and hydrophobic area, H (yellow); (Bellow) Separately presented main pharmacophore features of **3a** – topo II molecular recognition with the corresponding residues involved in this interaction and their interaction occurrence.

2.7. Cytotoxicity measurements of the 3,5-subtituted 1,2,4-oxadiazoles on the MCF-7 human breast cancer cell line

Encouraging results of the *in vitro* characterization of our oxadiazole compounds on the enzymatic topo IIα level stimulated us to investigate the cytotoxicity of the active synthesized compounds using the MTS assay and the MCF-7 human breast cancer cell line [42]. Selected human cancer cell line is representative and well-established systems for cell-based evaluation of potential anticancer compounds [42].

The initial screening of the synthesized derivatives was performed by exposing exponentially growing cells to a 100 μM concentration of the compounds for 72 h for compound **3a**, **3c**, **3e**, **3f**, **3j**, **4a**, **5a**, **5d, 5g, 5h, 12** and to a 50 μM for compounds **7**, **8, 10** and **11**. As a positive control, etoposide topo II poison (PC) was used. It was gratifying to observe that the first results revealed significant decrease of viability for four compounds **3a**, **7** and **11** along with the expected cytotoxicity of the PC. Results of the initial screening are represented in Figure 6.

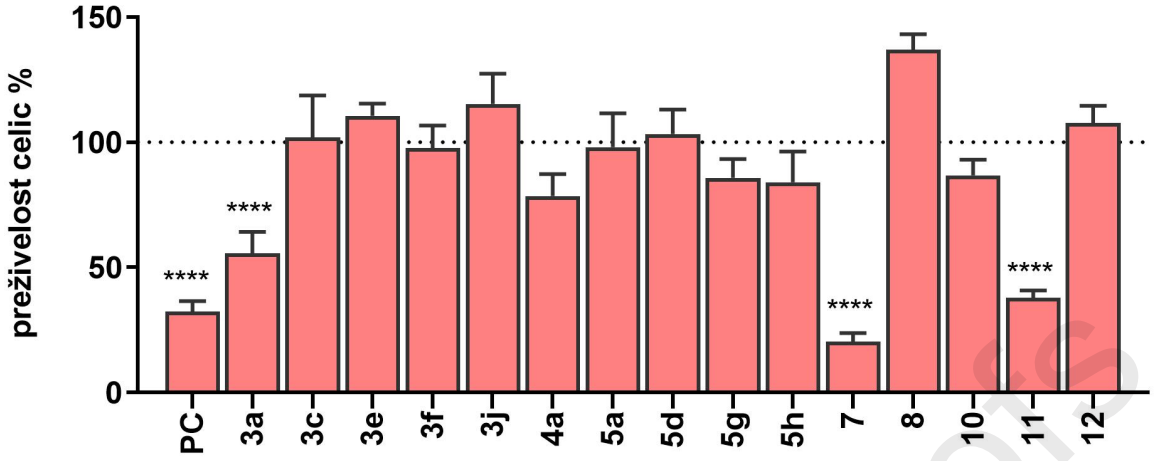

Figure 6. Results of the initial screening for cytotoxic activity of active 3,5-subtituted 1,2,4-oxadiazoles on the MCF-7 breast cancer cell line after 72h treatment. Compounds were tested at 100 μM, except compounds **7**, **8, 10** and **11** at 50 μM. Significant differences between the solvent control and treated cells were calculated using ANOVA (****$p<0.0001$).

Based on the promising initial MTS screening results, we selected compounds **3a** and **7** that all reduced the cell viability by more than 40% relative to the control for the EC_{50} determination. Obtained EC_{50} values were 38.5 μM for compound **3a** and 29.4 μM for compound **7**, while the determined EC_{50} value for etoposide on the MCF-7 cell line after 72h treatment was 12.6 μM. Obtained dose-response curves of log concentrations versus the percent of cell viability are represented on Figure 7 for investigated 3,5-subtituted 1,2,4-oxadiazoles. For etoposide reference these data are available in Figure S9. This result renders these compounds from the 3,5-subtituted 1,2,4-oxadiazoles in the comparable range of cytotoxic activity as the etoposide reference.

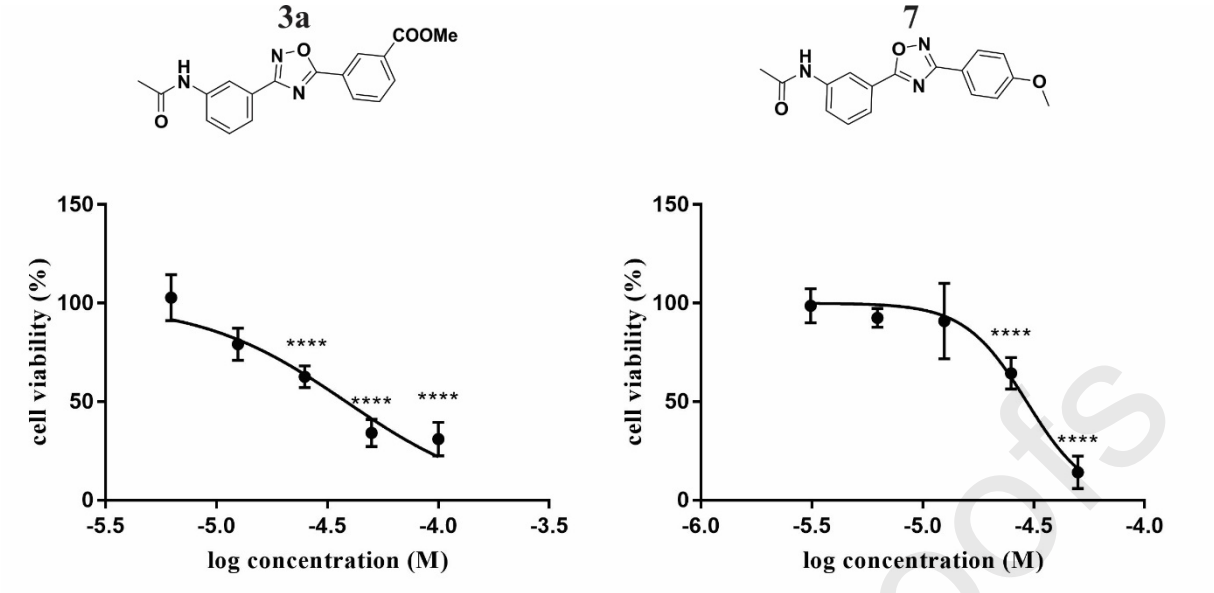

Figure 7. Dose-response curves of log concentrations versus percent viability for the 3,5-subtituted 1,2,4-oxadiazoles **3a** and **7** on the MCF-7 breast cancer cell line (72h treatment). Experiments were performed in five parallels and SD values were calculated. Significant differences between the solvent control and treated cells were calculated using ANOVA (****$p<0.0001$).

2.8. Analyses of the induction of the DNA double strand breaks by γ-H2AX assay

As we sought to gain more insight into the mechanism of action also on the molecular level we further investigated if this class of compounds causes the formation of the DNA double strand breaks (DSB) for the selective most characterized active oxadiazole compound **3a**. DSB are one form of the DNA damage that can lead to chromosomal breakage and rearrangement [55] and is related to severe side effects of topo II poisons, such as cardiotoxicity and induction of secondary malignancies [14, 16, 56]. With topo IIα-mediated cleavage assay presented in Section 2.4., we confirmed that the active compound **3a** acts via the catalytic inhibition and not as topo II poison on the molecular level. With the γ-H2AX assay developed to assess the compounds ability to induce the DNA double strand breaks [42], we aimed to confirm the same, but on the next molecular level of investigation.

Furthermore, we were particularly eager to proceed with these additional experiments since we observed that the MTS-determined values of cytotoxicity of active oxadiazole compounds were exhibiting even lower values compared to topo II inhibition. It is well known that *in vitro* enzymatic and cellular activity are challenging to correlate due numerous reasons such as differences in solubility, cell penetration and the intricate mode of action of any compound exercised on the molecular level [46].

The principle of the γ-H2AX assay uses the premise that the phosphorylated H2AX histones (γ-H2AX) can be used as biomarkers for the detection of DSB and DNA damage as they accumulate at sites, forming foci that correlate to DSB in a 1:1 ratio [57, 58]. Thus, the MCF-7 cells were exposed to compound **3a** at 10 and 50 μM concentrations for 72 h and then the assay was performed by flow cytometry measuring the fluorescent signals of the individual cells indirectly through the detection of the γ-H2AX foci. We were pleased to observe that the results revealed no statistically significant increase in the formation of DSBs after the 72h exposure of the MCF-7 cells to compound **3a** vs the solvent control. As expected, reference compound etoposide, an established topo IIα poison, did induce a statistically significant increase in DSB formation at 50 μM (Figure 8), which is in line with its proven mechanism of action at the molecular level. It is important to point out that such mechanism of action coupled with less additional DNA damage is also connected with the decreased likelihood of inducing additional secondary cellular injuries which can result in novel cancer pathologies. Nevertheless, it should be stressed that these results represent only a first promising indication and a subsequent preclinical investigation is necessary to fully evaluate the activity of these compounds at the cellular as well as molecular levels.

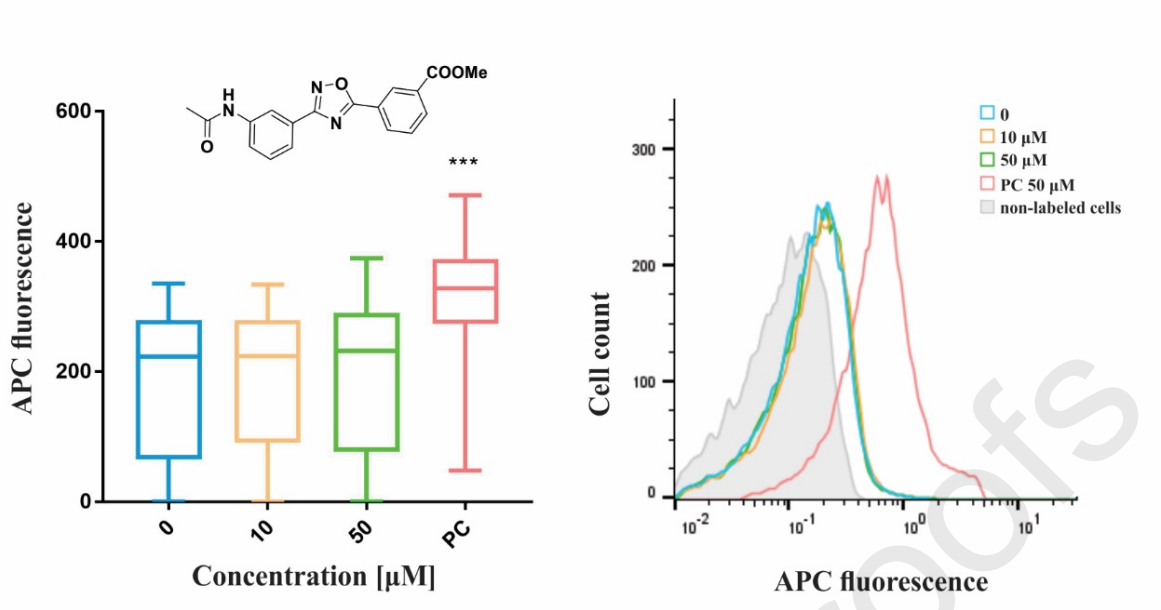

Figure 8. Results of the analyses of the induction of the DNA double strand breaks determined by γ-H2AX assay for the compound **3a**. (right) Distribution of the fluorescent signals of individual cells in the samples is shown. Data are presented as quantile box plots. The edges of the box represent the 25th and 75th percentiles, the median is a solid line through the box, and the bars represent 95% confidence intervals. In each sample, 10^4 events were recorded, and experiments were repeated three times independently. Significant difference between treated cells and the solvent control (0) is indicated by *** $p < 0.001$. A solvent control (0. 5% DMSO) and a positive control (50 µM etoposide) were included in each parallel. (Left) Representative histograms for vehicle control (0), compound **3a** at 10 µM and 50 µM, etoposide at 50 µM and non-labelled cells.

3. CONCLUSIONS

Cancer represents a broad and diverse group of diseases that are associated with abnormal cell growth which can potentially spread to other parts of the body and are one of the leading causes of death. Due to the known limitations of established topo II poisons such as cardiotoxicity, induction of secondary malignancies and recognized cancer cell resistance, an emerging group of catalytic topo II inhibitors is attempting to circumvent these challenges.

In this study we utilized a structure-based approach to design and discover a new chemical class of 3,5-substituted 1,2,4-oxadiazoles that can act as catalytic inhibitors of human topo IIα. By introducing the substituted rigid substitutions with additional functional groups on the oxadiazole core, it was possible to enhance the intermolecular interactions with the ATP binding site, especially in a part of the binding site where the " "triphospate" groups of the ATP molecule interact. We synthesized 25 new derivatives **3-6** of this chemical series and additionally tested 9 "reversely" substituted, commercially available 3,5-substituted 1,2,4-oxadiazoles **7-15**. The HTS topo IIα relaxation assay revealed that compounds **3a** and **10-12**, showed topo IIα inhibition in the micromolar range. Further investigations using the cleavage assay confirmed that the optimized series acts via a catalytic mechanism of topo IIα inhibition. The SPR binding experiments confirmed that such oxadiazoles (e.g. compound **3a**) can bind to the truncated ATPase domain, which is consistent with their targeted mode of action - binding to the ATPase domain. The predicted inhibitor **3a** binding geometries were evaluated using molecular dynamic (MD) simulations and dynophore models, outlining the importance of the Asn120 hydrogen bond along with the hydrophobic interactions of the two phenyl rings adjacent to the core oxadiazole moiety.

Several compounds of the series displayed cytotoxicity against the MCF-7 breast cancer cell line, with the activity closely comparable with the etoposide topo II standard inhibitor. Compound **3a** also did not induce DNA double-strand breaks (DSB) in this cancer cell line,

which in principle demonstrates a safer mechanism of action that is different from topo II poisons on the cellular level. The developed series of 3,5-substituted 1,2,4-oxadiazoles comprises compounds that are fully amenable for optimization and could pave the way for the development of future safer chemotherapies without the present harmful side of effects of topo II poisons such as cardiotoxicity, using the paradigm of catalytic inhibition.

4. EXPERIMENTAL SECTION

4.1. General chemistry methods

Reagents and solvents were obtained from various commercial sources (Acros Organics, Aldrich, TCI Europe, Merck, Alfa Aesar, Fluorochem). Solvents were distilled before use, while other chemicals were used as received. Reactions were monitored using a standard thin-layer chromatography plates (Merck 60 F254, 0.20 mm), and the components were visualized under UV light and/or through staining with the relevant reagent. Flash column chromatography was performed on Merck Silica Gel 60 (particle size 0.040-0.063 mm; Merck, Germany). NMR spectra (^{1}H and ^{13}C) were recorded using a Bruker Avance III 400 MHz spectrometer at 400 MHz for ^{1}H NMR and 100 MHz for ^{13}C NMR with magnet Bruker UltrashieldTM 400 PLUS at 298 K. As internal standard tetramethylsilane (TMS) was used, as solvent deuterated dimethyl sulfoxide (d6-DMSO) or deuterated chloroform ($CDCl_3$). Chemical shifts (δ) are reported in parts per million (ppm). The coupling constants (J) are provided in Hz, and the splitting patterns are designated as follows: s, singlet; br s, broad singlet; d, doublet; dd, double doublet; ddd, doublet of doublet of doublets; t, triplet; dq, doublet of quartets; qd, quartet of doublets; sept, septet; m, multiplet. Mass spectra data were performed on spectrometer Advion expression CMSL with ESI technique. High-resolution mass spectrometry (HR-MS) measurements were performed on spectrometer Q Exactive™ Plus Hybrid Quadrupole-Orbitrap™ (Thermo Fisher Scientific). HPLC analysis were performed with instrument Agilent Technologies HP 1100, with detector UV-VIS G1365B set to 254 nm and column Agilent Zorbax Eclipse Plus C18 (4.6 x 150 mm, 5 μm), which was thermostated at 25 °C using precolumn with flow rate 1 mL/min and a sample injection volume of 10 μL. As mobile phase acetonitrile (A) and 0.1% trifluoroacetic acid in water (B) was used. Percent of acetonitrile was changed with time: 0-16 min, 30% A, 70% B → 90% A, 10% B, 16-20 min 90% A, 10% B.

The purities of the test compounds used for the biological evaluations were >95%, as determined by HPLC (unless noted otherwise).

4.2. Synthetic experimental procedures and compounds characterization data

Synthesis of N-(3-cyanophenly)acetamide (IIa)

3-aminobenzonitrile (**Ia**) (7.146 g, 60.4 mmol) was dissolved in stirred solution of anhydrous methanol (390 mL) at room temperature. The solution of acetic anhydride (8 mL, 84.7 mmol) was added dropwise through a dropping funnel to the mixture above. After one hour of reaction, the solvent was evaporated under reduced pressure. Crude products were washed with cold water (40 mL) and obtained through the course of vacuum filtration.

*N-(3-cyanophenil)acetamide (**IIa**)*. Yield 98.52%; Brown crystals; Rf: 0.45 (MF: chloroform / methanol = 9:1); ^{1}H-NMR (400 MHz, DMSO-d6): δ [ppm] 2.08 (s, 3H, CH_3CO); 7.48-7.54 (m, 2H, 2H-Ar); 7.78 (d, 1H, J = 11.61 Hz, 1H-Ar); 8.09 (s, 1H, 1H-Ar); 10.30 (s, 1H, NH); IR (cm^{-1}): 3266, 2226, 1664, 1614, 1585, 1553, 1473, 1450, 1424, 1365, 1326, 1292, 1261, 1021, 895, 792, 752, 678, 624, 530; MS (ESI+): m/z 161.2 $[M+H]^+$; HR-MS: Calcd for $C_9H_9N_2O$ m/z: 161.0709 $[M+H]^+$, found 161.0711; Melting point: 106-110 °C

Synthesis of N-(4-cyanophenyl)acetamide (IIb)

4-aminobenzonitrile (**Ib**) (7.146 g, 60.4 mmol) was dissolved in stirred solution of anhydrous methanol (150 mL) at room temperature. The solution of acetic anhydride (27 mmol; 2.6 mL) was added dropwise through a dropping funnel to the mixture above. After one day, 0.6 mL of acetic anhydride was added. After 2 days, the mixture was evaporated and covered with water (20 mL) to which some ice was added. The precipitate was filtered off by suction and dried.

*N-(4-cyanophenyl)acetamide (**IIb**).* Yield: 90.18%; Yellow powder; Rf: 0.55 (MF: chloroform / methanol = 9/1); ^{1}H-NMR (400 MHz, DMSO-d6): δ[ppm] 2.09 (s, 3H, CH_3CO); 7.76 (s, 4H, 4H Ar); 8.08 (s, 1H, 1H Ar); 10.38 (s, 1H, NH); IR (cm^{-1}): 3307, 3250, 3182, 3107, 2217, 1665,

16596, 1529, 1505, 1403, 1360, 1320, 1264, 1175, 1014, 833, 818, 740, 602,543; MS (ESI-): m/z 158.99 $[M-H]^-$; Melting point: 155-157 °C

Synthesis of N-(3-(N'-hydroxycarbamimidoyl)phenyl) acetamide (IIIa)

Hydroxylammonium chloride (4.9 g; 64 mmol) was added to anhydrous ethanol (418 mL) under stirring condition, followed by triethylamine (9 mL; 64 mmol). The solution was stirred until everything was dissolved, followed by adding the compound **IIa** (9.4 g; 58.7 mmol). After addition of compound **IIa**, the reaction mixture was heated to reflux at 100 °C on/at oil bath for 24 hours. After 24 hours, another portion of hydroxylammonium chloride (1.5 g, 20 mmol) and triethyamine (3 mL, 20 mmol) was added to the reaction mixture. The reaction was left under reflux for another 48 hours under stirring condition. The process of the rection was detected through TLC method. After the reaction, the solvent was evaporated under reduced pressure. The obtained precipitate was washed with some ether and cold water and left for a few minutes on ice bath. The crude products were obtained by vacuum filtration.

*N-(3-(N'-hydroxycarbamimidoyl)phenyl)acetamide (**IIIa**).* Yield 63.19%; Light brown crystals; Rf: 0.21 (MF: chloroform / methanol = 9:1); ^{1}H-NMR (400 MHz, DMSO-d6): δ [ppm] 2.04 (s, 3H, CH_3CO); 5.73 (s, 2H, NH_2); 7.30 (s, 2H, 2H-Ar); 7.58-7.62 (m, 1H, H-Ar); 7.88 (s, 1H, H-Ar); 9.62 (s, 1H, OH); 9.98 (s, 1H, NH); IR (cm^{-1}): 3441, 3195, 1649, 1608, 1559, 1490, 1441, 1380, 1323, 1305, 1265, 981, 930, 872, 794, 766, 693, 682, 636, 604, 542; MS (ESI+): m/z 193.9 $[M+H]^+$; HR-MS: Calcd for $C_9H_{12}O_2N_3$ m/z: 194.0924 $[M+H]^+$, found 194.0926; Melting point: 74.4-73.5 °C

Synthesis of N-(4-(N'-hydroxycarbamimidoyl)phenyl)acetamide (IIIb)

Hydroxylammonium chloride (14.9 mmol; 1.04 g) was added to anhydrous ethanol (100 mL) under stirring condition, followed by triethylamine (14.9 mmol; 2.1 mL). After stirring until everything is dissolved (about 15 min) compound **IIb** (12.5 mmol; 2 g) was added and heated at boiling point (100 ° C). As the reaction proceeds slowly, 0.21 g of hydroxylammonium

chloride and 420 µL of triethylamine are added after 23 hours. After 48 hours, the reaction was completed, and the reaction mixture evaporated. A mixture of ice and water (75 mL) was then added and the precipitate formed was filtered off by suction and washed with a little ice water and dried.

*N-(4-(N'-hydroxycarbamimidoyl)phenyl)acetamide (**IIIb**)*. Yield: 94.07%; Yellowish powder; Rf: 0.13 (MF: chloroform / methanol = 9/1); ^{1}H-NMR (400 MHz, DMSO-d6): δ[ppm] 2.07 (s, 3H, CH_3CO); 5.74 (s, 2H, NH_2); 7.26- 7.58 (m, 4H, 4H Ar); 9.52 (s, 1H, OH); 10.03 (s, 1H, NH); IR (cm^{-1}): 3241, 1638, 1594, 1540, 1406, 1369, 1336, 1307, 1276, 1185, 958, 837, 814, 732, 685, 611, 571, 514; MS (ESI+): 193.95 $[M+H]^+$ (calculated 193.203); Melting point: 150-152 °C

General procedure for the synthesis of O-acylated amidoximes 1a-k

In anhydrous dichloromethane (35 mL) **compound IIIa** (1.01 mmol; 194.8 mg) was dissolved and reaction mixture was cooled to 0 °C. Triethylamine (1.26 mmol; 0.35 mL) was added. Appropriate amount of corresponding benzoyl chloride **IVa-j,** Table S4 (1.26 mmol) was then slowly added dropwise. After completion of the reaction (45 min from the start of acid chloride dropping), 15 mL of dichloromethane was added, and the mixture was transferred to a separating funnel. The organic phase was washed with water (3 x 20 mL) and saturated aqueous sodium chloride solution (20 mL). The dichloromethane was evaporated on a rotary evaporator. The precipitate formed was washed with cold water and obtained to crude products with vacuum filtration.

*Methyl-3-(((((3-acetamidophenyl)(amino)methylene)amino)oxy)carbonyl)benzoate **(1a)***. Yield: 45.56%; White powder; Rf: 0.54 (MF: chloroform / methanol = 9:1); ^{1}H-NMR (400 MHz, DMSO-d6): δ[ppm] 2.07 (s, 3H, CH_3CO); 3.92 (s, 3H, CH_3COO), 7.04 (s, 2H, NH_2); 7.40-7.42 (d, 2H, J = 5.1 Hz, 2H Ar); 7.70-7.74 (t, 1H, J = 8.2 Hz, 1H Ar); 7.80-7.83 (t, 1H, J = 4.7 Hz, 1H Ar); 7.95 (s, 1H, 1H Ar); 8.22-8.24 (d, 1H, J = 9.5 Hz, 1H Ar); 8.52-8.54 (d, 1H,

J = 8.3 Hz, 1H Ar); 8.61 (s, 1H, 1H Ar); 10.14 (s, 1H, NH); IR (cm^{-1}): 3579, 3470, 3316, 3255, 3088, 2953, 1732, 1711, 1681, 1632, 1596, 1578, 1561, 1484, 1447, 1437, 1401, 1369, 1299, 1235, 1192, 1166, 1129, 1100, 1088, 1071, 998, 976, 944, 921, 889, 823, 778, 726, 714, 653, 612, 582, 540, 504; MS (ESI-): m/z 353.97 $[M-H]^-$; HR-MS: Calcd for $C_{18}H_{18}N_3O_5$ m/z: 356.1238 $[M+H]^+$, found 356.1246; Melting point: 162-164 °C

Methyl-4-(((((3-acetamidophenyl)(amino)methylene)amino)oxy)carbonyl)benzoate ***(1b)***. Yield: 29.03%; White powder; Rf: 0.58 (chloroform / methanol = 9:1); ^{1}H-NMR (400 MHz, DMSO-d6): δ[ppm] 2.07 (s, 3H, CH_3CO); 3.92 (s, 3H, CH_3COO); 7.04 (s, 2H, NH_2); 7.35-7.43 (d, 2H, 2H Ar); 7.79-7.84 (m, 1H, 1H Ar); 7.94 (s, 1H, 1H Ar); 8.08-8.11 (d, 2H, J = 8.7 Hz, 2H Ar); 8.32-8.34 (d, 2H, J = 8.7 Hz, 2H Ar); 10.14 (s, 1H, NH); IR (cm^{-1}): 3423, 3208, 3080, 1726, 1711, 1676, 1639, 1602, 1582,1552, 1508, 1438,1408, 1371, 1316, 1280,1249, 1190, 1164, 1116, 1107,1083, 1020, 965, 920, 899, 889, 874, 853, 827, 799, 757, 722, 694, 672, 652, 616, 593, 531; MS (ESI-): m/z 353.91 $[M-H]^-$; HR-MS: Calcd for $C_{18}H_{16}N_3O_5$ m/z: 354.1080 $[M-H]^-$, found 354.1090; Melting point: 170-172 °C

N-(3-(N'-((3-chlorobenzoyl)oxy)carbamimidoyl)phenyl)acetamide ***(1c)***. Yield: 50%; White powder; Rf: 0.33 (MF: chloroform / methanol = 9:1); ^{1}H-NMR (400 MHz, DMSO-d6): δ[ppm] 2.06 (s, 3H, CH_3CO); 7.06 (s, 2H, NH_2); 7.56-7.58 (d, 2H, J = 7.93 Hz, 2H-Ar); 7.6 (s, 1H, 1H-Ar); 7.71 (s, 2H, 2H-Ar); 7.93 (s, 1H, 1H-Ar); 8.12-8.14 (d, 1H, J = 7.87 Hz, 1H-Ar); 8.26 (d, 1H, J = 3.48 Hz, 1H-Ar); 10.13 (s, 1H, 1H-Ar); IR (cm^{-1}): 3466, 3300, 1723, 1675, 1627, 1573, 1556, 1440, 1367, 1292, 1246, 1118, 1066, 1008, 872, 806, 742, 713, 668, 536; MS (ESI+): m/z 354.9 $[M+Na]^+$; HR-MS: Calcd for $C_{16}H_{15}ClN_3O_3$ m/z: 332.0796 $[M+H]^+$, found 332.0794; Melting point: 159-160.5 °C

N-(3-(N'-((4-chlorobenzoyl)oxy)carbamimidoyl)phenyl)acetamide ***(1d)***. Yield: 57%; White electrostatic powder; Rf: 0.35 (MF: chloroform / methanol = 9:1); ^{1}H-NMR (400 MHz, DMSO-d6): 2.06 (s, 3H, CH_3CO); 7.00 (s, 2H, NH_2); 7.39-7.41 (d, 2H, J = 5.3 Hz, 2H-Ar); 7.60-7.61

(d, 2H, J = 6.74 Hz, 2H-Ar); 7.78-7.81 (d, 1H, J = 15.35 Hz, 1H-Ar); 7.93 (s, 1H, 1H-Ar); 8.21-8.23 (d, 2H, J = 8.67 Hz, 2H-Ar); 10.13 (s, 1H, NH); IR (cm^{-1}): 33485, 3372, 3032, 1724, 1655, 1615, 1585, 1566, 1442, 1394, 1290, 1115, 1091, 1014, 910, 849, 795, 752, 716, 686, 531; MS (ESI-): m/z 329.7 $[M-H]^-$; HR-MS: Calcd for $C_{16}H_{15}ClN_3O_3$ m/z: 332.0796 $[M+H]^+$, found 332.0792; Melting point: 134-137.5 °C

N-(3-(N'-((3-(trifluoromethyl)benzoyl)oxy)carbamimidoyl)phenyl)acetamide ***(1e)***. Yield 72.2%; White crystals; Rf: 0.40 (MF: chloroform / methanol = 9:1); ^{1}H-NMR (400 MHz, DMSO-d6): δ [ppm] 2.07 (s, 3H, CH_3CO); 7.11 (s, 2H, NH_2); 7.42 (d, 2H, J = 18.08 Hz, 2H-Ar); 7.79-7.84 (m, 2H, H-Ar); 7.95 (s, 1H, H-Ar); 8.05-8.07 (d, 2H, J = 9.23 Hz, 2H-Ar); 8.45 (s, 1H, H-Ar); 8.50 (d, 2H, J = 7.84 Hz, H-Ar); 10.17 (s, 1H, NH); IR (cm^{-1}): 3663, 3466, 3084, 1731, 1677, 1628, 1600, 1580, 1562, 1445, 1336, 1296, 1242, 1163, 1125, 1072, 911, 882, 803, 748, 718, 693, 648, 609; MS (ESI+): m/z 366.1 $[M+H]^+$; HR-MS: Calcd for $C_{17}H_{15}N_3O_3F_3$ m/z: 366.1062 $[M+H]^+$, found 366.1058; Melting point: >340 °C

N-(3-(N'-((4-(trifluoromethyl)benzoyl)oxy)carbamimidoyl)phenyl)acetamide ***(1f)***. Yield 97.4%; White solid; Rf = 0.43 (MF: dichloromethane / methanol = 9:1); ^{1}H-NMR (400 MHz, DMSO-d6): δ [ppm] 2.07 (s, 3H, CH_3CO); 7.06 (s, 2H, NH_2); 7.41 (d, 2H, J = 4.84 Hz, 2H-Ar); 7.78-7.83 (m, 1H, H-Ar); 7.92 (t, 3H, J = 8.5 3H-Ar); 8.40 (d, 2H, J = 8.1 Hz, 2H-Ar); 10.14 (s, 1H, NH); IR (cm^{-1}): 3489, 1728, 1657, 1619, 1585, 1567, 1441, 1321, 1291, 1269, 1181, 1137, 1096, 1065, 1017, 860, 795, 769, 704, 513; MS (ESI+): m/z 366.0 $[M+H]^+$; HR-MS: Calcd for $C_{17}H_{15}N_3O_3F_3$ m/z: 366.1062 $[M+H]^+$, found 366.1057; Melting point: 153.0-154.8 °C

N-(3-(N'-((3-methoxybenzoyl)oxy)carbamimidoyl)phenyl)acetamide ***(1g)***. Yield: 79%; White powder; Rf: 0.47 (MF: chloroform / methanol = 5:1); ^{1}H-NMR (400 MHz, DMSO-d6): δ [ppm] 2.07 (s, 3H, CH_3CO); 3.86 (s, 3H, CH_3O); 6.96 (s, 2H, NH_2); 7.40 (d, 2H, 2H Ar); 7.22-7.26 (d, 1H, 1H Ar); 2.40-2.48 (m, 3H, 3H Ar); 7.65 (s, 1H, 1H Ar); 7.66-7.84 (d, 2H, 2H Ar); 7.93

(s, 1H, 1H Ar); 10.14 (s, 1H, NH); IR (cm^{-1}): 3485, 3417, 3153, 1723, 1639, 1598, 1570, 1442, 1378, 1327, 12296, 1270, 1218, 1182, 1100, 1068, 1032, 871, 799, 747, 706, 677, 617, 589, 549; MS (ESI-): m/z 325.8 $[M-H]^-$; HR-MS: Calcd for $C_{17}H_{18}N_3O_4$ m/z: 328.1292 $[M+H]^+$, found 328.1287; Melting point: 87-89 °C

N-(3-(N'-((4-methoxybenzoyl)oxy)carbamimidoyl)phenyl)acetamide ***(1h)***. Yield: 67%; White powder; Rf: 0.6 (MF: chloroform / methanol = 9:1); ^{1}H-NMR (400 MHz, DMSO-d6): δ [ppm] 2.07 (s, 3H, CH_3CO); 3.86 (s, 3H, CH_3O); 6.91 (s, 2H, NH_2); 7.37-7.41 (d, 2H, J = 17.37, 2H-Ar); 7.78-7.83 (d, 1H, J = 19.29, 1H-Ar); 7.93 (s, 1H, 1H-Ar); 8.15-8.17 (d, 2H, J = 8.93, 2H-Ar); 10.15 (s, 1H, NH); IR (cm^{-1}): 3489, 1697, 1670, 1632, 1602, 1580, 1538, 1443, 1390, 1253, 1173, 1082, 1020, 861, 764, 697, 607; MS (ESI+): m/z 327.9 $[M+H]^+$; HR-MS: Calcd for $C_{17}H_{18}N_3O_4$ m/z: 328.1292 $[M+H]^+$, found 328.1288; Melting point: 153-155.5 °C

N-(3-(N'-((4-nitrobenzoyl)oxy)carbamimidoyl)phenyl)acetamide ***(1i)***. Yield 88%; White-yellowish solid; Rf: 0.35 (MF: chlorofom / methanol = 9:1); ^{1}H-NMR (400 MHz, DMSO-d6): δ [ppm] 2.08 (s, 3H, CH_3CO); 7.12 (s, 2H, NH_2); 7.40 (d, 1H, J = 5.11 Hz, H-Ar); 7.98 (s, 1H, H-Ar); 8.35 (d, 2H, J = 9.01 Hz, 2H-Ar); 8.46 (d, 2H, J = 9.03 Hz, 2H-Ar); 10.30 (s, 1H, NH); IR (cm^{-1}): 3471,0; 3267,7; 1722,4; 1672,7; 1634,0; 1605,4; 1585,5; 1550,7; 1523,7; 1444,6; 1401,6; 1349,7; 1324,6; 1272,1; 1093,5; 1015,3; 915,9; 873,3; 858,5; 800,5; 779,2; 710,1; 641,6; 610,3; 533,2; 510,3; MS (ESI-): m/z 341.0 $[M-H]^-$; HR-MS: Calcd for $C_{16}H_{15}O_5N_4$ m/z: 343.1037 $[M+H]^+$, found 343.1033; Melting point: 74-79 °C

N-(3-(N'-((3-fluoro-5-(trifluoromethyl)benzoyl)oxy)carbamimidoyl)phenyl)acetamide ***(1j)***. Yield 66%; White solid; Rf: 0.39 (MF: chloroform / methanol = 9:1); ^{1}H-NMR (400 MHz, DMSO-d6): δ [ppm] 2.07 (s, 3H, CH_3CO); 7.17 (s, 2H, NH_2); 7.40-7.44 (m, 2H, 2H-Ar); 7.80 (d, 2H, J = 11.27 Hz, 2H-Ar); 7.93 (s, 1H, H-Ar); 8.06 (d, 2H, J = 7.94 Hz, 2H-Ar); 8.27 (s, 1H, H-Ar); 8.41 (d, 2H, J = 7.8 Hz, 2H-Ar); 10.15 (s, 1H, NH); IR (cm^{-1}): 3478, 3296, 3092, 1731, 1680, 1629, 1601, 1573, 1544, 1440, 1357, 1254, 1238, 1193, 1164, 1132, 1106, 881,

760, 691,639, 595, 538; MS (ESI-): 381.8 $[M-H]^-$; HR-MS: Calcd for $C_{17}H_{14}O_3N_3F_4$ m/z: 384.0966 $[M+H]^+$, found 348.0961; Melting point: 100-104 °C

General procedure for the synthesis of O-acylated amidoximes 2a-b

Compound **IIIb** (1.00 mmol;) was dissolved in anhydrous dichloromethane (35 mL) and mixture cooled to 0 °C. Then triethylamine (1.26 mmol; 0.35 mL) was added and appropriate benzoyl chloride (1.01 mmol); was slowly added dropwise. After completion of the reaction (45 min from the start of acid chloride dripping), 15 mL of dichloromethane was added, and the mixture was transferred to a separating funnel. The organic phase was washed with water (3 x 20 mL) and saturated aqueous sodium chloride solution (20 mL). The dichloromethane was evaporated on a rotary evaporator.

Methyl-3-(((((4-acetamidophenyl)(amino)methylene)amino)oxy)carbonyl)benzoate ***(2a)***.

Yield: 40.2%; White powder; Rf: 0.51 (MF: chloroform / methanol = 9:1); ^{1}H-NMR (400 MHz, DMSO-d6): δ[ppm] 2.09 (s, 3H, CH_3CO); 3.92 (s, 3H, CH_3COO), 6.97 (s, 2H, NH_2); 7.66-7.75 (m, 5H, 5H Ar); 8.21-8.24 (d, 1H, J = 10.8 Hz, 1H Ar); 8.50- 8.52 (d, 1H, J = 8.8 Hz, 1H Ar); 8.60 (s, 1H, 1H Ar); 10.17 (s, 1H, NH); IR (cm^{-1}): 3085, 2924, 2855, 1725, 1675, 1607, 1530, 1410, 1372, 1296, 1249, 1184, 1096, 1032, 1011, 967, 926, 841, 723, 675, 577; MS (ESI-): 353.94 $[M-H]^-$; HR-MS Calcd for $C_{18}H_{18}N_3O_5$ m/z: 356.1251 $[M+H]^+$, found 356.1246; Melting point: 120-123 °C

Methyl-4-(((((4-acetamidophenyl)(amino)methylene)amino)oxy)carbonyl)benzoate ***(2b).***

Yield: 51.93%; Light brown solid; Rf: 0.51 (chloroform / methanol = 9:1); ^{1}H-NMR (400 MHz, DMSO-d6): δ[ppm] 2.07 (s, 3H, CH_3CO); 3.92 (s, 3H, CH_3COO), 6.97 (s, 2H, NH_2); 7.40-7.42 (m, 4H, 4H Ar); 8.08-8.104 (d, 2H, J = 8.7 Hz, 2H Ar); 8.31- 8.33 (d, 2H, J = 8.7 Hz, 2H Ar); 10.17 (s, 1H, NH); IR (cm^{-1}): 3454, 3296, 3168, 1745, 1720, 1669, 1638, 1608, 1543, 1442, 1407, 1379, 1332, 1310,1284, 1248, 1190, 1117, 1105, 1078, 1016, 959, 922, 868, 857, 840,

790, 719, 686, 675, 627, 576, 542; MS (ESI-): m/z 353.94 $[M-H]^-$; HR-MS Calcd for $C_{18}H_{16}N_3O_5$ m/z: 354.1085 $[M-H]^-$, found 354.1090; Melting point: 170-172 °C

Procedures for the cyclization reaction

Appropriate amount of corresponding **O-acylated amidoxime (1a-j**, **2a-2b)** was dissolved in the solution of anhydrous toluene. The reaction was heated to boiling point for 10 days for compounds **3c**, **3h**, 8 days for compound **3f**, 7 days for compound **3e** and **3d**, 6 days for compound **3a** and **4b,** 5 days for compound **4a**, **3g**, **3i** and **3j**, 3 days for compound **3b** under stirring condition. The process of reaction was detected through TLC method. After the reaction, the precipitated product was obtained through the course of vacuum filtration.

*Methyl 3-(3-(3-acetamidophenyl)-1,2,4-oxadiazol-5-yl)benzoate (**3a**).* Yield: 46.35%; Yellow powder; Rf: 0.56 (MF: chloroform / methanol = 9:1); ^{1}H-NMR (400 MHz, DMSO-d6): δ[ppm] 2.10 (s, 3H, CH_3CO); 3.96 (s, 3H, CH_3COO); 7.52-7.56 (t, 1H, J =15.9 Hz, 1H Ar); 7.78 (d, 1H, 1H Ar); 7.88 (t, 2H, 2H Ar); 8.29-8.33 (t, 1H, J = 16.3 Hz, 1H Ar); 8.42-8.47 (t, 2H, J = 9.6 Hz, 2H Ar); 8.70 (s, 1H, 1H Ar); 10.25 (s, 1H, NH); ^{13}C-NMR (75MHz, CDCl3): δ[ppm] 24.67, 52.60, 118.66, 122.77, 123.19, 124.62, 127.37, 129.30, 129.41, 129.76, 131.29, 132.13, 133.58, 138.58, 165.98, 168.63, 168.71, 174.84 ; IR (cm^{-1}): 3270, 3111, 1727, 1664, 1618, 1597, 1564, 1441, 1346, 1288,1245, 1168, 1132, 1104, 1000, 962, 887, 802, 737, 709, 681, 609, 565, 537; MS (ESI+): m/z 338.1 $[M+H]^+$; HR-MS Calcd for $C_{18}H_{16}N_3O_4$ m/z: 338.1142 $[M+H]^+$, found 338.1141; HPLC: compound purity 100% at 254 nm (t_R = 8.3 min); Melting point: 123-126 °C

*Methyl 4-(3-(3-acetamidophenyl)-1,2,4-oxadiazol-5-yl)benzoate (**3b**).* Yield: 32.82%; White powder; Rf: 0.53 (MF: chloroform / methanol = 9:1); ^{1}H-NMR (400 MHz, DMSO-d6): δ[ppm] 2.10 (s, 3H, CH_3CO); 3.94 (s, 3H, CH_3COO); 7.54 (t, 1H, 1H Ar); 7.78 (m, 1H, 1H Ar); 7.88 (t, 2H, 2H Ar); 8.25 (d, 1H, 1H Ar); 8.34 (d, 2H, 2H Ar); 8.44 (s, 1H, 1H Ar); 10.26 (s, 1H, NH); IR (cm^{-1}): 3364, 3120, 2606, 2362, 1716, 1656, 1562, 1519, 1490, 1423, 1366, 1350,

1316, 1284, 1240, 1185, 1108, 1050, 1018, 972, 927, 888, 845, 786, 763, 744, 692, 668, 609, 574, 537; MS (ESI-): m/z 336.09 $[M-H]^-$; HR-MS Calcd for $C_{18}H_{15}N_3O_4$ m/z: 336.0898 $[M-H]^-$, found 336.0998; HPLC: compound purity 95.12% at 254 nm (t_R = 8.5 min); Melting point: 200-202 °C;

N-(3-(5-(3-chlorophenyl)-1,2,4-oxadiazol-3-yl)phenyl)acetamide ***(3c)***. Yield: 74%; White powder; Rf: 0.63 (MF: chloroform / methanol = 9:1); ^{1}H-NMR (400 MHz, DMSO-d6): δ [ppm] 2.09 (s, 3H, CH_3CO); 7.47-7.54 (m, 1H, 1H-Ar); 7.69-7.80 (m, 2H, 2H-Ar); 7.80-7.84 (m, 2H, 2H-Ar); 8.14-8.18 (m, 2H, 2H-Ar); 8.41 (s, 1H, 1H-Ar); 10.23 (s, 1H, NH); ^{13}C-NMR (75 MHz, $CDCl_3$): δ[ppm] 24.52; 117.79; 122.09; 122.38; 125.74; 126.78; 127.08; 127.86; 130.24; 132.10; 133.61; 134.64; 140.57; 168.80; 169.14; 174.67**;** IR (cm^{-1}): 3264, 3113, 1758, 1662, 1558, 1460, 1443, 1408, 1344, 1325, 1290, 1128, 1019, 968, 883, 799, 771, 749, 675, 560, 536; MS (ESI-): 312.8 $[M-H]^-$; HR-MS Calcd for $C_{16}H_{13}ClN_3O_2$ m/z**:** 314.0691 $[M+H]^+$, found 314.0683; HPLC: compound purity 100% at 254 nm (t_R = 6.9 min); Melting point: 175-177 ºC

N-(3-(5-(4-chlorophenyl)-1,2,4-oxadiazol-3-yl)phenyl)acetamide ***(3d).*** Yield: 56%; beige crystals; Rf: 0.47 (MF: chloroform / methanol = 9:1); ^{1}H-NMR (400 MHz, DMSO-d6): δ [ppm] 2.09 (s, 3H, CH_3CO); 7.50-7.54 (m, 1H, 1H-Ar), 7.74-7.82 (m, 4H, 4H-Ar), 8.19-8.21 (m, 2H, 2H-Ar), 8,41 (s, 1H, 1H-Ar); 10,23 (s, 1H, NH); ^{13}C-NMR (75 MHz, $CDCl_3$): δ[ppm] 24.52; 117.78; 122.07; 122.34; 122.72; 123.29; 126.86; 130.20; 138.68; 140.57; 168.79; 169.12; 175.04; IR (cm^{-1}): 3319, 1669, 1601, 1581, 1561, 1508, 1477, 1406, 1368, 1278, 1216, 1094, 1014, 843, 804, 757, 720, 694, 689, 534; MS (ESI+): 313.9 $[M+H]^+$; HR-MS Calcd for $C_{16}H_{13}ClN_3O_2$ m/z 314.0691 $[M+H]^+$, found 310.687; HPLC: compound purity 100 % at 254 nm (t_R = 6.9 min); Melting point: 184-186 ºC

N-(3-(5-(3-(trifluoromethyl)phenyl)-1,2,4-oxadiazol-3-yl)phenyl)acetamide ***(3e)****:* Yield 88%; White crystals; Rf: 0.47 (MF: chloroform / methanol = 9:1); ^{1}H-NMR (400 MHz, DMSO-d6): δ [ppm] 2.09 (s, 3H, CH_3CO); 7.53 (t, 1H, J = 7.96 Hz, H-Ar); 7.78 (d, 1H, J = 8.03, H-Ar);

7.83 (d, 1H, J = 9.11 Hz, H-Ar); 7.94 (t, 1H, J = 7.88 Hz, H-Ar); 8.14 (d, 1H, J = 8.58 Hz, H-Ar); 8.43 (s, 1H, H-Ar); 8.49 (d, 2H, J = 7.87 Hz, 2H-Ar); 10.28 (s, 1H, NH); ^{13}C (75 MHz, DMSO-d6): 24.50, 117.81, 122.06, 122.42, 124.72, 124.93, 126.70, 130.20, 130.48, 130.80, 131.53, 132.35, 140.55, 168.86, 196.19, 174.63; IR (cm^{-1}): 3304, 1656, 1596, 1547, 1511, 1465, 1441, 1348, 1331, 1317,1287, 1271, 1160, 1116, 1100, 1072, 1020, 910, 883, 803, 757, 710, 694, 532; MS (ESI-): 345.9 $[M-H]^-$; HR-MS Calcd for $C_{17}H_{13}O_2N_3F_3$ m/z: 348.0954 $[M+H]^+$, found 348.0954; HPLC: compound purity 98.48% at 254 nm (t_R = 6.843 min); Melting point: 165-170 °C

*N-(3-(5-(4-(trifluoromethyl)phenyl)-1,2,4-oxadiazol-3-yl)phenyl)acetamid) **(3f)***. Yield 81%; White solid; Rf: 0.47 (MF: dichloromethane / methanol = 9:1); ^{1}H-NMR (400 MHz, DMSO-d6): δ [ppm] 2.10 (s, 3H, CH_3CO); 7.53 (t, 1H, J = 7.96 Hz, H-Ar); 7.77 (d, 1H, J = 8.03 Hz, H-Ar); 7.81 (d, 1H, J=8.16 Hz, H-Ar); 8.05 (d, 2H, J = 8.26 Hz, 2 H-Ar); 8.39 (d, 2H, J = 8.1 Hz, 2H-Ar); 8.43 (s, 1H, H-Ar); 10.24 (s, 1H, NH);^{13}C (75 MHz, DMSO-d6): 24.51, 117.79, 122.07, 122.40, 122.74, 125.45, 126.73, 126.99, 127.53, 129.32, 140.60, 168.91, 196.14, 174.69; IR (cm^{-1}): 1662, 1551, 1467, 1448, 1419, 1346, 1319, 1292, 1164, 1118, 1087, 1064, 1018, 867, 761, 736, 710, 691, 679, 532; MS (ESI-): 345.9 $[M-H]^-$ (calculated: 347.2972); HR-MS Calcd for $C_{17}H_{13}O_2N_3F_3$ m/z: 348.0954 $[M+H]^+$**,** found 348.0951; HPLC: compound purity 99.51% at 254 nm (t_R = 6.957 min); Melting point: 187-190 °C

N-(3-(5-(3-methoxyphenyl)-1,2,4-oxadiazol-3-yl)phenyl)acetamide (***3g*).** Yield: 74%; White powder; Rf: 0.58 (MF: chloroform / methanol = 9:1); ^{1}H-NMR (400 MHz, DMSO-d6): δ [ppm] 2.10 (s, 3H, CH_3CO); 3.90 (s, 3H, CH_3O); 7.30-7.33 (d, 1H, J = 10.27 Hz, 1H-Ar); 7.50-7.65 (m, 3H, 3H-Ar), 7, 76-7.78 (m, 3H, 3H-Ar), 8.38 (s, 1H, 1H-Ar), 10.24 (s, 1H, 1H-Ar); ^{13}C-NMR (75 MHz, $CDCl_3$): δ[ppm] 24.50; 56.0; 112.85; 117.79; 120.0; 120.69; 122.32; 124.98; 126.95; 130.20; 131.38; 140.56; 160.18; 168.74; 169.15; 175.75; IR (cm^{-1}): 3311, 1669, 1599, 1561, 1509, 1492, 1410, 1371, 1283, 1220, 1042, 877, 857, 805, 760, 740, 679; MS (ESI-):

307.9 $[M-H]^-$; HR-MS Calcd for $C_{17}H_{16}N_3O_3$ m/z: 310.1186 $[M+H]^+$, found 310.1182; HPLC: compound purity 100% at 254 nm (t_R = 6.4 min); Melting point: 154-156 °C

N-(3-(5-(4-methoxyphenyl)-1,2,4-oxadiazol-3-yl)phenyl)acetamide ***(3h).*** Yield: 96%; White powder; Rf: 0.46 (MF: chloroform / methanol = 9:1); ^{1}H-NMR (400 MHz, DMSO-d6): δ [ppm] 2.09 (s, 3H, CH_3CO); 3.89 (s, 3H, CH_3O); 7.19-7.22 (d, 2H, J = 8.93 Hz, 2H-Ar); 7.49-7.53 (t, 1H, J = 15.87 Hz, 1H-Ar); 7.81(s, 1H, 1H-Ar); 7.83 (s, 1H, 1H-Ar); 8.12-8.14 (d, 2H, J = 8.9 Hz, 2H-Ar); 8.38 (s, 1H, 1H-Ar); 10.26 (s, 1H, NH); ^{13}C-NMR (75 MHz, $CDCl_3$): δ[ppm] 24.51; 56.13; 115.49; 117.78; 122.04; 122.20; 127.17; 130.15; 140.53; 163.60; 168.57; 169.12; 175;73; IR (cm^{-1}): 3274, 1659, 1610, 1541, 1511, 1444, 1349, 1311, 1251, 1187, 1110, 1080, 1022, 887, 838, 800, 708, 683m 619; MS (ESI-): 307.7 $[M-H]^-$; HR-MS Calcd for $C_{17}H_{16}N_3O_3$ m/z: 310.1186 $[M+H]^+$, found 310.1183; HPLC: compound purity 100% at 254 nm (t_R = 6.2 min); Melting point: 175-178 °C

N-(3-(5-(4-nitrophenyl)-1,2,4-oxadiazol-3-yl)phenyl)acetamide ***(3i)****.* Yield 24%; Yellowish solid; Rf: 0.57 (MF: chloroform / methanol = 9:1); ^{1}H-NMR (400 MHz, DMSO-d6): δ [ppm] 2.61 (s, 3H, CH_3CO); 7.54 (t, 1H, J = 7.80 Hz, H-Ar); 7.77-7.89 (m, 2H, 2H-Ar); 8.43-8.52 (m, 5H, 5H-Ar); 10.25 (s, 1H, CONH); ^{13}C (75 MHz, DMSO-d6): 24.42, 119.51, 121.73, 123.24, 128.84, 129.45, 130.81, 130.23, 139.15, 147.96, 147.96, 169.90, 166.72, 175.85; IR (cm^{-1}): 3572, 1668, 1598, 1562, 1518, 1462, 1443, 1401, 1376, 1336, 1295, 1226, 1108, 1015, 854, 808, 771, 740, ; 708, 685, 663, 614, 538; MS (ESI+): 325.1 $[M+H]^+$; HR-MS Calcd for $C_{16}H_{13}O_4N_4$ m/z: 325,0931 $[M+H]^+$, found 325.0930; HPLC: compound purity 97.76% at 254 nm (t_R = 6.2 min); Melting point: 53.3-55.1 °C

N-(3-(5-(3-fluoro-5-(trifluoromethyl)phenyl)-1,2,4-oxadiazol-3-yl)phenyl)acetamide ***(3j)****.* Yield 77.8%; Orange powder; Rf: 0.51 (MF: chloroform / methanol = 9:1); ^{1}H-NMR (400 MHz, DMSO-d6): δ [ppm] 2.07 (s, 3H, CH_3CO); 7.52 (t, 1H, J = 7.94 Hz, H-Ar); 7.78 (d, 1H, J=6.72 Hz, H-Ar); 7.83 (d, 1H, J=9.17 Hz, H-Ar); 8.16 (d, 1H, J = 8.32 Hz, H-Ar); 8.72 (s, 1H, H-Ar);

8.32 (d, 1H, J=8.44 Hz, H-Ar); 8.40 (s, 1H, H-Ar); ^{13}C (75 MHz, DMSO-d6): 24.49, 117.76, 119.46, 119.70, 121.16, 127.16, 122.10, 122.46, 126.52, 127.08, 127.16, 130.25, 140.60, 161.49, 163.97, 168.92, 173.71; IR (cm^{-1}): 1660, 1600, 1573, 1468, 1434, 1362, 1327, 1280, 1267, 1242, 1170, 1134, 1082, 924, 886, 796, 758, 703, 693, 540; MS (ESI-): 364.0 $[M-H]^-$; HR-MS Calcd for $C_{17}H_{12}O_2N_3F_4$ m/z: 366.0862 $[M+H]^+$, found 366.0858; HPLC: compound purity 94.52% at 254 nm (t_R = 6.983 min); Melting point: 102-106 °C

*Methyl 3-(3-(4-acetamidophenyl)-1,2,4-oxadiazol-5-yl)benzoate (**4a**)*. Yield: 79.63%; Brown powder; Rf: 0.36 (chloroform / methanol = 15:1); ^{1}H-NMR (400 MHz, DMSO-d6): δ[ppm] 2.11 (s, 3H, CH_3CO); 3.95 (s, 3H, CH_3COO); 7.80-7.87 (m, 5H, 5H Ar); 8.28-8.31 (d, 1H, 1H Ar); 8.44-8.47 (d, 1H, 1H Ar); 8.29-8.33 (d, 1H, 1H Ar); 8.70 (s, 1H, 1H Ar); 10.29 (s, 1H, NH); ^{13}C-NMR (75 MHz, $CDCl_3$): δ[ppm] 23.75, 51.35, 51.54, 118.57, 121.32, 123.66, 127.49, 127.58, 128.23, 128.36, 130.24, 130.26, 131.14, 132.51, 132.79, 133.20, 139.63, 164.93, 167.55, 173.69; IR (cm^{-1}): 3315, 2963, 1722, 1676, 1605, 1547, 1527, 1479, 1435, 1412, 1363, 1295, 1252, 1178, 1100, 996, 962, 925, 841, 723, 599, 518; MS (ESI-): 335.94 $[M-H]^-$; HR-MS Calcd for $C_{18}H_{16}N_3O_4$ m/z: 338.1146 $[M+H]^+$, found 338.1141; HPLC: compound purity 96.71% at 254 nm (t_R = 8.3 min); Melting point: 180-183 °C

*Methyl 4-(3-(4-acetamidophenyl)-1,2,4-oxadiazol-5-yl)benzoate (**4b**)*. Yield: 37.99%; White powder; Rf: 0.36 (chloroform / methanol = 15:1); ^{1}H-NMR (400 MHz, DMSO-d6): δ[ppm] 2.10 (s, 3H, CH_3CO); 3.92 (s, 3H, CH_3COO); 7.80-7.83 (d, 2H, J = 8.8 Hz, 2H Ar); 8.04-8.06 (d, 2H, J = 8.8 Hz, 2H Ar); 8.21-8.23 (d, 2H, J = 8.7 Hz, 2H Ar); 8.32-8.34 (d, 2H, J = 8.7 Hz, 2H Ar); 10.29 (s, 1H, NH); IR (cm^{-1}): 3120, 2830, 2608, 1707, 1656, 1562, 1487, 1418, 1316, 1284, 1240, 1185, 1111, 1050, 974, 926, 843, 786, 763, 741, 697, 668, 610; MS (ESI-): 335.95 $[M-H]^-$; HR-MS Calcd for $C_{18}H_{14}N_3O_4$ m/z: 336.0987 $[M-H]^-$, found 336.0984; HPLC: compound purity 97.12% at 254 nm (t_R = 8.9 min); Melting point: 95-98 °C

General procedure for the hydrolysis of esters 3a, 3b, 4a and 4b

Appropriate amount of the corresponding compound (**3a**, **3b**, **4a** or **4b**) was dissolved in 20 mL of dioxane. In the solution was then added appropriate amount of 2 M sodium hydroxide solution allowing to stir for 3 days at room temperature. After completion of the reaction, the solvent was evaporated; the residue was dissolved in 15 mL of water and washed with 15 mL of ethyl acetate. The aqueous phase was acidified with 5 M hydrochloric acid to pH 4 and extracted with ethyl acetate. The organic phase is then washed twice with 15 mL of water and 15 mL of saturated sodium chloride solution, dried with sodium sulfate, filtered and the solvent evaporated and continued with purification with ether.

*3-(3-(3-acetamidophenyl)-1,2,4-oxadiazol-5-yl)benzoic acid (**5a**)*. Yield: 61.73%; Light brown powder; Rf: 0.31 (MF: dichloromethane / methanol = 5:1 + 2% acetic acid); ^{1}H-NMR (400 MHz, DMSO-d6): δ[ppm] 2.10 (s, 3H, CH_3CO); 7.50-7.56 (t, 1H, 1H Ar); 7.78-7.88 (m, 3H, 3H Ar); 8.26-8.29 (d, 1H, J = 9.4 Hz, 1H Ar); 8.41-8.44 (s, 2H, 2H Ar); 8.70 (s, 1H, 1H Ar); 10.24 (s, 1H, NH); 13.54 (s, 1H, COOH); ^{13}C (75 MHz, DMSO-d6): 24.15; 119.51;120.89; 123.72; 126.10; 129.42; 130.31; 130.82; 131.42; 132.12; 139.01; 166.79; 168.90; 174.82; IR (cm^{-1}): 3272, 2833, 2534, 2350, 2172, 1681, 1605, 1555, 1505, 1405, 1370, 1271, 1082, 1022, 898, 802, 696, 551; MS (ESI-): 321.8 $[M-H]^-$; HR-MS Calcd for $C_{17}H_{12}N_3O_4$ m/z: 322.0822 $[M-H]^-$, found 322.0828; HPLC: compound purity 96.79% at 254 nm (t_R = 5.1 min); Melting point: 233-235 °C

*4-(3-(3-acetamidophenyl)-1,2,4-oxadiazol-5-yl)benzoic acid (**5b**)*. Yield: 12.65%; Brown solid; Rf: 0.31 (MF: dichloromethane / methanol = 5:1 + 2% acetic acid); ^{1}H-NMR (400 MHz, DMSO-d6): δ[ppm] 1.24 (s, 3H, CH_3CO); 7.51-7.55 (t, 1H, 1H Ar); 7.83-7.84 (m, 2H, 2H Ar); 8.15 (s, 1H, 1H Ar); 8.25-8.27 (m, 3H, 3H Ar); 8.42 (s, 1H, 1H Ar); 10.24 (s, 1H, NH); 13.54 (s, 1H, COOH); IR: 3120, 1675, 1540, 1508, 1410, 1380, 1260, 1081, 1060, 896, 775, 656, 575; MS (ESI-): 321.89 $[M-H]^-$; HR-MS Calcd for $C_{17}H_{12}N_3O_4$ m/z: 322.0828 $[M-H]^-$, found 322.0829; HPLC: Compound purity 95.10% at 254 nm (t_R = 4.9 min); Melting point:> 300 °C

*3-(3-(4-acetamidophenyl)-1,2,4-oxadiazol-5-yl)benzoic acid (**6a**)*. Yield: 31.75%; Yellow powder; Rf: 0.35 (MF: dichloromethane / methanol = 5:1 + 2% acetic acid); ^{1}H-NMR (400 MHz, DMSO-d6): δ[ppm] 2.10 (s, 3H, CH_3CO); 7.80-7.84 (m, 3H, 3H Ar); 8.05-8.07 (d, 2H, J = 8.8 Hz 2H Ar); 8.25-8.27 (d, 1H, J = 8.2 Hz, 1H Ar); 8.41-7.43 (d, 1H, J = 8 .4 Hz, 1H Ar); 8.68 (s, 1H, 1H Ar); 10.28 (s, 1H, NH); ^{13}C-NMR (75 MHz, DMSO-d6): δ[ppm] 24.13, 113.53, 119.02, 120.18, 123.86, 127.96, 128.43, 130.16, 131.81, 132.02, 133.58, 142.32, 166.21, 167.99, 168.79, 174.44; IR (cm^{-1}): 3280, 2824, 2552, 1675, 1604, 1529, 1479, 1415, 1353, 1299, 1178, 1108, 1020, 926, 846, 717, 674, 594, 509; MS (ESI-): 322.06 $[M-H]^-$; HR-MS Calcd for $C_{17}H_{12}N_3O_4$ m/z: 322.0827 $[M-H]^-$, found 322.0828; HPLC: compound purity 96.01% at 254 nm (t_R = 4.7 min); Melting point: 238-240 °C

*4-(3-(4-acetamidophenyl)-1,2,4-oxadiazol-5-yl)benzoic acid (**6b**)*. Yield: 34.36%; Yellow powder; Rf: 0.36 (dichloromethane / methanol = 5:1 + 2% acetic acid); ^{1}H-NMR (400 MHz, DMSO-d6): δ[ppm] 1.23 (s, 3H, CH_3CO); 7.80-7.82 (d, 2H, J=8,8 Hz, 2H Ar); 8.04-8.06 (d, 2H, J = 8.8 Hz, 2H Ar); 8.18-8.20 (d, 2H, J = 8.1 Hz, 2H Ar); 8.29- 8.31 (d, 2H, J = 8.5 Hz, 2H Ar); 10.29 (s, 1H, NH); 13.45 (s, 1H, COOH); ^{13}C-NMR (75 MHz, DMSO- d6): δ[ppm] 24.14, 119.05, 120.16, 126.73, 127.96, 128.15, 130.27, 142.36, 168.09, 168.82, 174.50; IR (cm^{-1}): 2923, 2361, 2339, 1684, 1606, 1586, 1556, 1525, 1503, 1471, 1412, 1365, 1317, 1291, 1183, 1136, 1113, 1076, 1018, 971, 928, 868, 841, 751, 723, 693, 633, 604, 554, 522; MS (ESI-): 321.89 $[M-H]^-$; HR-MS Calcd for $C_{17}H_{12}N_3O_4$ m/z: 322.0828 $[M-H]^-$, found 322.0821; HPLC: compound purity 98.51% at 254 nm (t_R = 4.7 min); Melting point: 277-279 °C

General procedure for the hydrolysis of the amide bond for compounds 3a, 3c-3j

A stirred mixture of appropriate amount of corresponding 3,5-disubstited 1,2,4-oxadiazoles (1.0 mmol) and 5M HCl (2 mL; 10 mmol) in tetrahydrofuran (16 mL) was heated to reflux at 76 °C for 30 h. After the reaction, the THF was evaporated under reduced pressure. 20 mL of distilled

water was added to the mixture in the flask, followed by slowly dropping 10 M NaOH to alkaline and adjust the pH to 10.0. The precipitated product was filtered by vacuum.

*3-(5-(3-chlorophenyl)-1,2,4-oxadiazol-3-yl)aniline (**5c**).* Yield: 97%, White powder; Rf: 0.78 (MF: chloroform / methanol = 9:1); ^{1}H-NMR (400 MHz, DMSO-d6): δ [ppm] 5.56 (s, 2H, NH_2); 6.77-6.83 (d, 1H, J = 25.15 Hz, 1H-Ar); 7.20-7.26 (d, 2H, J = 23.44 Hz, 2H-Ar); 7.33-7.35 (d, 1H, J = 28.58 Hz, 1H-Ar); 7.69-7.73 (m, 1H, 1H-Ar); 7.81-7.84 (d, 1H, J = 11.29, 1H-Ar); 8.13-8.17 (m, 2H, 2H-Ar); ^{13}C-NMR (75MHz, $CDCl_3$): δ[ppm] 112.4, 114.87, 117.48, 125.88, 126.83, 127.01, 127.81, 130.19, 132.07, 133.49, 134.63, 149.83, 169.43, 174.32; IR (cm^{-1}): 3334, 1612, 1596, 1558, 1461, 1434, 1409, 1356, 1314, 1259, 1069, 875, 800, 770, 746, 672, 572, 542; MS (ESI+): 271.8 $[M+H]^+$; HR-MS Calcd for $C_{14}H_{11}ClN_3O$ m/z: 272.0585 $[M+H]^+$, found 272.0583; HPLC: compound purity 100% at 254 nm (t_R = 5.5 min); Melting point: 131-133 ºC

*3-(5-(4-chlorophenyl)-1,2,4-oxadiazol-3-yl)aniline (**5d**)*. Yield: 94%; White flakes; Rf: 0.7 (MF: chloroform / methanol = 9:1); ^{1}H-NMR (400 MHz, DMSO-d6): δ [ppm] 5.47 (s, 2H, NH_2); 6.75-6.80 (d, 1H, J = 17,83 Hz, 1H-Ar); 7.21-7.24 (d, 2H, J = 10.45 Hz, 2H-Ar); 7.33 (s, 1H, 1H-Ar); 7.74-7.76 (d, 2H, J = 8.71 Hz, 2H-Ar); 8.17-8.19 (d, 2H, J = 8.7 Hz, 2H-Ar); ^{13}C-NMR (75 MHz, $CDCl_3$): δ[ppm] 112.40; 114.84; 117.43; 122.85; 126.91; 130.14; 130.22; 138.54; 149.85; 169.32; 174.70; IR (cm^{-1}): 3364, 1611, 1488, 1465, 1405, 1358, 1270, 1093, 1015, 874, 840, 796, 752, 680, 577, 537; MS (ESI+): 272.0 $[M+H]^+$; HR-MS Calcd for $C_{14}H_{11}ClN_3O$ m/z: 272.0585 $[M+H]^+$, found 272.0581; HPLC: compound purity 100% at 254 nm (t_R = 5.4 min); Melting point: 142-144 ºC

*3-(5-(3-(trifluoromethyl)phenyl)-1,2,4-oxadiazol-3yl)aniline (**5e**).* Yield 65.5%; Light brown crystals; Rf: 0.64 (MF: chloroform / methanol = 9:1); ^{1}H-NMR (400 MHz, DMSO-d6): δ [ppm] 5.45 (s, 2H, NH_2); 6.79 (d, 1H, J = 11.43 Hz, H-Ar); 7.21-7.29 (m, 2H, 2H-Ar); 7.38 (s, 1H, H-

Ar); 7.93 (t, 1H, J= 7.87 Hz, H-Ar); 8.13 (d, 1H, J = 7.91 Hz, H-Ar); 8.41 (s, 1H, H-Ar); 8.47 (d, 1H, J = 7.85 Hz, H-Ar); ^{13}C (75 MHz, DMSO-d6): 112.46, 114.83, 117.47, 122.68, 124.67, 125.06, 125.38, 126.77, 130.20, 130.48, 130.80, 131.49, 149.88, 169.39, 174.90; IR (cm^{-1}): 3584, 3330, 1626, 1566, 1461, 1362, 1326, 1301, 1258, 1236, 1168, 1127, 1098, 1070, 910, 875, 814, 754, 726, 711, 687, 648, 613, 571, 540; MS (ESI+): 306.2 $[M+H]^+$; HR-MS Calcd for $C_{15}H_{11}ON_3F_3$ m/z: 306.0843 $[M+H]^+$, found 306.0843; HPLC: compound purity 93.24% at 254 nm (t_R = 5.517 min); Melting point: 85-87 °C

*3-(5-(4-(trifluoromethyl)phenyl)-1,2,4-oxadiazol-3-yl)aniline (**5f**).* Yield 67.8%; Beige solid; Rf: 0.62 (MF: chloroform / methanol = 9:1); ^{1}H-NMR (400 MHz, DMSO-d6): δ [ppm] 5.60 (s, 2H, NH_2); 6.83 (d, 1H, J = 11.4 Hz, 2H-Ar); 7.23-7.30 (m, 2H, 2H-Ar); 7.40 (s, 1H, H-Ar); 8.05 (d, 2H, J = 8.26 Hz, 2H-Ar); 8.38 (d, 2H, J = 8.1 Hz, 2H-Ar); ^{13}C (75 MHz, DMSO-d6): 112.91, 115.44, 117.98, 122.76, 125.47, 126.82, 127.66, 129.27, 130.28, 149.07, 169.39, 174.40; IR (cm^{-1}): 1567, 1463, 1360, 1318, 1168, 1124, 1111, 1083, 1063, 1017, 875, 852, 799, 760, 737, 701, 682, 591, 573; MS (ESI+): 306.0 $[M+H]^+$; HR-MS Calcd for $C_{15}H_{11}ON_3F_3$ m/z: 306.0849 $[M+H]^+$, found 306.0844; HPLC: compound purity 96.48% at 254 nm (t_R = 5.540 min); Melting point: 86-86 °C

*3-(5-(3-methoxyphenyl)-1,2,4-oxadiazol-3-yl)aniline (**5g**).* Yield: 87%; Powder beige; Rf: 0.36 (MF: chloroform / methanol = 9: 1); ^{1}H-NMR (400 MHz, DMSO-d6): δ [ppm] 3.86 (s, 3H, CH_3O); 5.65 (s, 2H, NH_2); 6.78-6.83 (m, 1H, 1H-Ar); 7.22-7.24 (d, 2H, J = 7.29 Hz, 2H-Ar); 7.26-7.28 (m, 1H, 1H-Ar); 7.32-7.36 (m, 1H, 1H-Ar); 7.57-7.59 (m, 1H, 1H-Ar); 7.61-7.65 (m, 1H, 1H-Ar), 7.75-7.77 (m, 1H, 1H-Ar); ^{13}C-NMR (75 MHz, $CDCl_3$): δ[ppm] 55.99; 112.42; 112.80; 114.84; 117.37; 119.87; 120.62; 125.11; 127.0; 130.16; 131.15; 149.85; 160.18; 169.28; 175.41; IR (cm^{-1}): 3436, 1565, 1493, 1461, 1356, 1318, 1283, 1221, 1041, 989, 875, 852, 795, 682, 573, 536; MS (ESI-): 265.9 $[M-H]^-$; HR-MS Calcd for $C_{15}H_{14}N_3O_2$ m/z:

268.1081 $[M+H]^+$, found 268.1074; HPLC: compound purity 96.48% at 254 nm (t_R = 4.8 min); Melting point: 101-102.5 °C

*3-(5-(4-methoxyphenyl)-1,2,4-oxadiazol-3-yl)aniline (**5h**).* Yield: 98%; Brownish powder; Rf: 0.35 (MF: chloroform / methanol = 9:1); ^{1}H-NMR (400 MHz, DMSO-d6): δ [ppm] 3.89 (s, 3H, OCH_3), 6.97-7.00 (m, 1H, 1H-Ar), 7.19-7.22 (m, 2H, 2H-Ar), 7.32-7.35 (t, 1H, J = 26.19 Hz, 1H-Ar), 7.43-7.45 (m, 1H, 1H-Ar), 7.52-7.53 (m, 1H, 1H-Ar), 8.11-8.13 (m, 2H, 2H-Ar); ^{13}C-NMR (75 MHz, $CDCl_3$): δ[ppm] 56.13; 115.49; 116.23; 118.64; 120.24, 127.51; 130.36; 130.50; 144.71; 163.57; 168.67; 175.61; IR (cm^{-1}): 3402, 3319, 1611, 1585, 1526, 1501, 1485, 1424, 1368, 1307, 1253, 1176, 1118, 1018. 872, 832, 756, 724, 679, 636, 620, 548, 515; MS (ESI+): 267.8 $[M+H]^+$; HR-MS Calcd for $C_{15}H_{14}N_3O_2$ m/z: 268.1081 $[M+H]^+$, found 268.1074; HPLC: compound purity 100% at 254 nm (t_R = 4.7 min); Melting point: 102-106 °C

*3-(5-(4-nitrophenyl)-1,2,4-oxadiazol-3yl)aniline (**5i**).* Yield 41.5%; Orange solid; Rf: 0.66 (MF: chloroform / methanol = 9:1); ^{1}H-NMR (400 MHz, DMSO-d6): δ [ppm] 5.50 (s, 2H, NH_2); 6.77-6.81 (m, 1H, H-Ar); 7.21-7.26 (m, 2H, 2H-Ar); 7.35 (s, 1H, H-Ar); 8.46 (dd, 4H, J_1 = 9.1 Hz, J_2 = 13.78 Hz, 4H-Ar);^{13}C-NMR (75 MHz, DMSO-d6): 112.39, 114.83, 117.55, 125.09, 126.67, 129.31, 129.84, 130.23, 149.89, 150.37, 169.56, 173.96; IR (cm^{-1}): 3374, 1628, 1593, 1563, 1513, 1467, 1334, 1277, 1107, 856, 794, 768, 737, 708, 683, 573, 547, 521; MS (ESI-): 280.9 $[M-H]^-$; HR-MS Calcd for $C_{14}H_{11}O_3N_4$ m/z: 283.0826 $[M+H]^+$, found 283.0822; HPLC: compound purity 75.11% at 254 nm (t_R = 4.620 min); Melting point: 40.5-42.7 °C

*3-(5-(3-fluoro-5-(trifluoromethyl)phenyl)-1,2,4-oxadiazol-3-yl)aniline (**5j**).* Yield 62.5%; Brown powder; Rf : 0.67 (MF: chloroform / methanol = 9:1); ^{1}H-NMR (400 MHz, DMSO-d6): δ [ppm] 5.53 (s, 2H, NH_2); 6.79 (d, 1H, J = 9.24 Hz, H-Ar); 7.20-7.27 (m, 2H, 2H-Ar); 7.36 (s, 1H, H-Ar); 8.16 (d, 1H, J = 8.58 Hz, H-Ar); 8.27 (s, 1H, H-Ar); 8.32 (d, 1H, J=8.55 Hz, H-Ar);^{13}C (75 MHz, DMSO-d6): 112.4, 114.85, 117.96, 118.66, 119.67, 121.12, 126.58, 127.32,

130.21, 149.90, 161.50, 163.90, 169.47, 173.36; IR (cm^{-1}): 3357, 3221, 1597, 1573, 1464, 1434, 1369, 1337, 1280, 1264, 1204, 1176, 1129, 1099, 1084, 1008, 922, 887, 795, 816, 757, 689, 577, 535, 519; MS (ESI+): 324.2 $[M+H]^+$; HR-MS Calcd for $C_{15}H_{10}ON_3F_4$ m/z: 324.0755 $[M+H]^+$, found 324.0751; HPLC: compound purity 82.13% at 254 nm (t_R = 5.703 min); Melting point: 56-60 °C

*Methyl 3-(3-(3-aminophenyl)-1,2,4-oxadiazol-5-yl)benzoate (**5k**).* Yield 71.16%; Brown solid; Rf: 0.65 (MF: chloroform / methanol = 9:1); ^{1}H-NMR (400 MHz, DMSO-d6): δ [ppm] 3.95 (s, 3H, CH_3COO); 5.48 (s, 2H, NH_2); 6.78 (d, 1H, J = 9.19 Hz, H-Ar); 7.20-7.29 (m, 1H, H-Ar); 7.37 (s, 1H, H-Ar); 7.84 (t, 2H, J = 7.84 Hz, H-Ar); 8.28 (d, 1H, J = 0.57 Hz, H-Ar); 8.43 (s, 1H, H-Ar); 8.68 (s, 1H, H-Ar); ^{13}C (75 MHz, DMSO-d6): 51.55, 114.29, 117.83, 118.90, 126.35, 129.95, 130.20, 130.60, 131.40, 131.82, 148.90, 163.51, 169.41, 174.88; IR (cm^{-1}): 2919, 1726, 1615, 1596, 1563, 1463, 1434, 1359, 1299, 1248, 1136, 1103, 1085, 957, 876, 796, 709, 681, 574, 532; MS (ESI+): 296.1 $[M+H]^+$; HR-MS Calcd for $C_{16}H_{14}O_3N_3$ m/z: 296.1030 $[M+H]^+$, found 296.1028; HPLC: compound purity 88.47% at 254 nm (t_R = 4.650 min); Melting point: 44-47 °C

4.3. Molecular docking calculations

The molecular docking experiments were performed using GOLD software [33] and the human topo IIα ATPase domain (PDB: 1ZXM) [59]. In the first step, the validation of GOLD docking tool was performed [60] similarly to our previous studies [27, 29, 30] by redocking a native ligand AMP-PNP molecule into its binding site.

To summarize, the active site was defined as 10 Å radius around the reference ligand AMP-PNP and hydrogen atoms were added to the protein. Magnesium ion and all waters were removed except for W924 and W931. They were included in docking calculations because it was previously assumed that they play an important role in the binding of the AMP-PNP molecule [23]. AMP-PNP molecule was docked into the defined active site by applying the

following parameters of the GOLD genetic algorithm (GA): Population size=100, Selection pressure = 1.1, No. of Operations = 100000, No of Islands = 5, Niche size = 2, Migrate = 10, Mutate = 95, Crossover = 95. Different spin states of the water molecules W924 and W931 were allowed during docking procedure. As in previous studies to insure that interactions similar to the interaction pattern of the purine moiety in the AMP-PNP molecule would be obtained, a pharmacophore constrain to Asn120 was added [59] and GoldScore scoring function was used. Obtained binding pose of docked AMP-PNP closely resembled the experimentally determined, with the best RMSD agreement of 0.9 Å what indicated that used docking setting are reliable (Figure S1).

The same scoring function and the described docking settings were used for the molecular docking calculations of the designed 3,5-bisubtituted-1,2,4 oxadiazoles as well as commercially available reversely substituted compounds. All docking calculations were visualized and geometrically analyzed in LigandScout [34].

4.4. Molecular dynamics simulation and dynophore calculations

Molecular Dynamics (MD) simulations using a monomer of the human topo IIα ATPase domain (PDB: 1ZXM) with the docked conformations of the active oxadiazole compound **3a** was performed using CHARMM molecular modeling suite [61] applying our developed methodology.

The bound conformations in the ATP binding site were generated as described in previous section using GOLD molecular docking suite. The crystal structure of the protein was prepared and then simulated in a similar fashion as described previously [27, 29-31]. CHARMM-GUI environment was utilized for the protein manipulation and construction of the solvated protein-compound **3a** complexes [62]. CHARMM parameter and topology files (version 36) were utilized to specify the force field parameters of the amino acid residues comprising the protein [63, 64]. CHARMM General Force Field (CGenFF) was used to describe the atom types and

partial charges of active compound **3a** [65]. The 1,2,4 oxadiazole scaffold is a week base was thus modeled in its unprotonated form [66]. Determined partial charges and assigned atom types for these compounds are listed in the Supplementary material (Table S5). The protein-ligand system was immersed into a sphere TIP3 of water molecules [67] with truncated octahedral shape with the edge distance of 10 Å and 3 chlorine ions were added to make the system electroneutral. Ion placement was performed using a Monte Carlo method. The periodic boundary conditions (PBC) were applied based on the shape and size of the system. Grid information for the Particle-mesh Ewald (PME) Fast Fourier Transform (FFT) was generated automatically. The final system prepared for the MD simulation was comprised of 73 274 atoms. Short energy minimizations were then performed to remove bad contacts. The system was then minimized for 10 000 steps by steepest descent (SD) method followed by 10 000 steps of modified Adopted Basis Newton–Raphson (ABNR) method and an MD equilibration run of 1 ns. Production MD trajectory was generated using leapfrog integration scheme and 2 fs simulation step using SHAKE algorithm. A 20 ns long MD simulation production run was performed. Conformations were sampled every 500th step resulting in 10 000 conformations for subsequent analysis. Visualization and analysis of the geometry parameters of the production MD trajectory was performed using VMD program [68]. RMSD was calculated against the initial docking conformation, taking all atoms into account. Overall conformational behavior of **3a** during the MD simulation can also be observed in the generated movie animation (see Supporting information, Animation).

To further provide a more comprehensive outlook of the observed interaction pattern and flexibility between the simulated ligand **3a** and the htIIα ATP binding site, 1000 exported MD equidistant frames were used in the dynamic pharmacophore analysis using DynophoreApp developed in the Molecular Design Lab at Freie Universität (FU) Berlin [48-50]. These calculations resulted in a dynophore models. These dynophore calculations were performed on

computers of the Molecular Design Lab, Berlin, Germany and subsequently visualized in LigandScout [34].

4.5. HTS relaxation assay of human topo IIα

The HTS topo IIα relaxation assay was performed on the black streptavidin-coated 96-well microtiter plate. Plate was rehydrated using wash buffer (20 mM Tris–HCl (pH = 7.6), 137 mM NaCl, 0.005% (w/v) BSA, 0.05% (v/v) TWEEN-20®) and biotinylated oligonucleotide was immobilized onto the wells. Next, the excess oligonucleotide was washed off with wash buffer. Enzyme assay was carried out in reaction volume of 30 µL using 0.75 µg supercoiled plasmid pNO1 as a substrate and human topo IIα. Enzyme was diluted to the appropriate concentration with dilution buffer comprised of 50 mM Tris-HCl (pH = 7.5), 100 mM NaCl, 1 mM DTT, 0.5 mM EDTA, 50% (v/v) glycerol and 50 µg/mL albumin. Tested compounds (0.3 µL) were added as a stock solution in DMSO and final concentration of DMSO was 1%, respectively. Reactions were incubated at 37 °C for 30 min, and TF buffer (50 mM NaOAc (pH = 5.0), 50 mM NaCl, 50 mM $MgCl_2$) was added to the wells and incubated at room temperature for additional 30 min to allow the triplex biotin-oligonucleotid-plasmid formation [38]. To eliminate the aggregation and non-specific inhibition a surfactant (TWEEN-20®) was added to the reaction mixture [69]. Unbound plasmid was washed off with TF buffer and stained with the DNA-detection Dye in the T10 buffer (10 mM Tris–HCl (pH = 8) and 1 mM EDTA) was added. After mixing, fluorescence was read using Tecan fluorimeter (Excitation: 485 nm and Emission: 535 nm). Screening was performed at the inhibitor concentrations of 7.8, 31.5, 125 and 500 µM for compounds **3a**, **3b**, **3i**, **4a**, **4b**, **5a**, **5b**, **5e**, **5f**, **5i**, **5j, 5k, 6a**, **6b, 7, 8, 9, 10, 11, 13, 14, 15** and 7.8, 62.5, 125, 250 µM for compounds **3c**, **3d**, **3e**, **3f**, **3g**, **3h**, **3j**, **5c**, **5d**, **5g**, **5h**, **12, etoposide.** IC_{50} values were calculated using GraphPad Prism 7.0 software [70] and represent the concentrations of inhibitors where residual activity of the enzyme was 50% [38]. Commercially available compounds possessing human topo IIα activity, were additionally characterized by

HRMS and the obtained spectra along with the NMR data are provided in the Supplementary information. LogP [40] and TPSA [41] values were calculated using ChemDraw Professional 16.0 (see Table S7).

4.6. The human topo IIα mediated cleavage assay

The human topo IIα cleavage assay was performed in collaboration with Inspiralis (Norwich, UK). One U of human topo IIα was incubated with the 0.5 μg supercoiled plasmid DNA (pBR322) and the respective amount of selected active compound **3a** or reference compound etoposide in a 30 μL reaction at 37 °C for 60 minutes under the following conditions: 20 mM Tris HCl (pH 7.5), 200 mM NaCl, 0.25 mM EDTA and 5% glycerol. Compound **3a** was tested at four concentrations: 3.9, 31.25, 125 and 500 μM. The reaction was then incubated for additional 30 minutes with 0.2% SDS and 0.5 μg/μL proteinase K. Subsequently, the reaction was stopped by adding 30 μL of chloroform/iso-amyl alcohol (26:1) and 30 μL of Stop Dye (40% sucrose (w/v), 100 mM Tris.HCl (pH 7.5), 10 mM EDTA, 0.5 μg/mL bromophenol blue), before sample being loaded on the 1% TAE gel run at 80 V for 2 hours.

Bands were visualized by the ethidium bromide staining for 15 minutes and destaining for subsequent 10 minutes. Gels were scanned using the documentation equipment (GeneGenius, Syngene, Cambridge, UK) and cleavage levels were calculated from the band data obtained by the gel scanning software (GeneTools, Syngene, Cambridge,UK).

4.7. SPR binding experiments using the isolated human topo IIα ATPase domain

Surface plasmon resonance (SPR) experiments were performed at 25 °C using a Biacore T100 (Biacore, GE Healthcare) instrument. Using a standard amino coupling method, human topo IIα ATPase was immobilized on the second flow cell of a CM5 sensor chip. The human topo IIα ATPase domain (fragment containing residues 1–453 with a His tag) was purchased from Inspiralis [71]. The carboxymethylated dextran layer was activated with a 720 seconds pulse of EDC (1-ethyl-3-(3-dimethylethylaminopropyl)-carbodiimide) and NHS (N-

hydroxysuccinimide) in a 1:1 ratio. Human topo IIα ATPase, diluted to a final concentration of 50 mg/mL in 10 mM sodium acetate (pH 6.0), was injected to reach a final immobilization level of 6200 units. The rest of the surface was deactivated with a 450 seconds injection of ethanolamine. The first flow served as a reference cell for subtraction of nonspecific binding and was activated with EDC/NHS and deactivated with ethanolamine. The system was reprimed with a new running buffer (10 mM HEPES pH 7.4, 150 mM NaCl, 3 mM EDTA, 0.005% surfactant P20). Analyte – compound **3a** was prepared as 50 mM stock solutions in DMSO and were diluted with running buffer (10 mM HEPES pH 7.4, 200 mM NaCl, 3 mM EDTA, 0.005% surfactant P20, 0.1 mg/mL BSA). Analyte was injected at a flow rate of 30 mL/min for 60 seconds, and dissociation was monitored for an additional 60 seconds [72]. Regeneration was provided with 2.5 mM NaOH for 8 seconds. To diminish the difference in the refractive index between samples and running buffer for the titration of analytes, 5% (v/v) DMSO was added to the running buffer. Compound **3a** was tested at six different concentrations (1.56, 3.13, 6.25, 12.5, 50, 100 μM) in three parallel titrations. Some concentrations were injected several times to check reproducibility. Sensorgrams were analysed using Biacore T100 Evaluation Software (Biacore, GE Healthcare). Equilibrium binding responses were determined from the binding levels 5 sec before stopping the injections, and finally, KD values were determined using Biacore T100 Evaluation Software software by fitting the data to Steady State Affinity model. We used solvent correction method to adjust measured responses for the effects of varying concentrations of DMSO.

4.8. *In vitro* cytotoxicity measurements using MTS assay on MCF-7 cell line

In vitro cytotoxicity of investigated compounds **3a**, **3c**, **3e**, **3f**, **3j**, **4a**, **5a**, **5d**, **5g**, **5h**, **7**, **8**, **10**, **11** and **12** was evaluated in the breast cancer MCF-7 cell line. The MCF-7 (ATCC) were cultivated in Eagle's MEM medium (M5650, Sigma), supplemented with 10% fetal bovine serum, 2 mM glutamine, and 100 IU/mL penicillin/streptomycin. After the cell exposure to the

tested compounds the viability of the MCF-7 was determined by MTS tetrazolium reduction assay.

The cells were seeded onto the 96-well microplates (Nunc, TermoFisher Scientific, Waltham, MA, USA) at densities of 7000 cells per well in 200 mL growth medium and incubated overnight to attach. The next day, the growth medium was replaced by the fresh complete growth medium containing appropriate concentrations of the compounds. Prepared microplates were then incubated for 72 h and subsequently 40 μL of freshly prepared MTS: PMS solution (20:1) was added directly to the 200 μL of medium in the culture wells and incubated for additional 3h (37 °C, 5% CO_2). Finally, the absorbance was measured at wavelength of 490 nm using a Microplate Reader (Synergy MX, BioTek, Winooski, VT, USA). As positive control, etoposide at 200 μM was used. Cell viability was determined by comparing the OD (optical density) of the wells containing the cells treated with investigated compounds with solvent control cells those of unexposed cells and presented as % of cell viability ± SD. The initial screening of the synthesized derivatives was performed by exposing exponentially growing cells to a 100 μM concentration of the compounds for 72 h for compound **3a**, **3c**, **3e**, **3f**, **3j**, **4a**, **5a**, **5d, 5g, 5h, 12** and to a 50 μM for compounds **7**, **8, 10** and **11.** For selected compounds, titrations were prepared. Compound **3a** was titrated at 6.25, 12.5, 25, 50, and 100 μM, compound **7** at 3.125, 6.25, 12.5, 25 and 50 μM Experiments were performed at least three times independently each time at five replicates. EC_{50} values were calculated by non-linear regression analysis using GraphPad Prism 7.0 Software. Statistical significance between treated groups and the control was determined by One-way analysis of variance and Dunnett's Multiple Comparison Test.

4.9. Analyses of the induction of DNA double strand breaks by γ-H2AX assay

The MCF-7 cells were seeded on the 25 cm^2 plates (Corning Inc.,NY, USA) (550 000 cells/plate), left to attach overnight and were subsequently exposed to the selected compound

3a (10 μM and 50 μM) and etoposide (positive control, 50 μM) for 72 h. After exposure the floating and adherent cells were collected by trypsinization. For the fixation, the cells were centrifuged at 1000 rpm, 4 °C for 5 min, washed twice with ice cold PBS, resuspended in 0.5 mL cold PBS and ethanol (1.5 mL) was added drop wise while vortexing. The cells were fixed at 4 °C overnight and stored at -20 °C until analysis. Fixed cells were centrifuged at 1200 rpm for 10 min, washed with ice cold 1 X PBS and labelled with Anti-H2AX pS139 antibodies according to manufacturer's protocol (Miltenyi Biotec, Germany). Flow cytometric analysis was carried out on a MACSQuant Analyzer 10 (Miltenyi Biotech, Germany). APC intensity, corresponding to DSBs, was detected in the APC-A channel. Unspecific binding was checked with rea-APC antibodies (Miltenyi Biotec, Germany). In each sample, 10 000 events were recorded. Independent experiments were repeated three times. In all experiments, 50 μM etoposide was included as positive control and 0.5% DMSO as solvent control. For further analysis, the raw data (APC intensities of each cell obtained as APC-A values) was exported from MACSQuantify software. Statistical analysis was performed with R statistic program, freely available on the web.

5. ACKNOWLEDGEMENT

This work was supported by the Ministry of Education, Science and Sport of the Republic of Slovenia through the Research program grants P1-0012, P1-0208 and P1-0245 as well as a Young Researcher Grant to K.B. Drs. Nicolas Burton and Alison Howells from Inspiralis, Norwich, UK are acknowledged for performing the human DNA topoisomerase IIα cleavage assay. Sara Bavcon, Santina Jazbinšek and Mojca Klemenčič, all M.Pharm., are acknowledged for synthesizing several oxadiazole compounds discussed in this work at the Faculty of

Pharmacy, University of Ljubljana. Matej Janežič M.Pharm, from the Structural Bioinformatics Team, Division of Structural and Synthetic Biology, Center for Life Science Technologies, RIKEN, Japan is thanked for stimulating discussions in the initial stage of this work. Prof. Žiga Jakopin from the Faculty of Pharmacy in is thanked for his assistance with HPLC analysis. Gregor Bajc, M.Sc. from the Infrastructural Centre from Molecular Interactions Analysis in Ljubljana, Slovenia, is thanked for technical help with the SPR measurements.

6. SUPPLEMENTARY MATERIAL

Supporting information associated with this article such additional docking figures, MD details MD animations, biochemical binding, and cell-based data as well as commercially available compounds analytical data can be found online.

7. REFERENCES

[1] National Cancer Institute, https://www.cancer.gov/about-cancer/understanding/statistics, (2018.02.26).

[2] D. Hanahan, R.A. Weinberg, The hallmarks of cancer, Cell, 100 (2000) 57-70.

[3] D. Hanahan, R.A. Weinberg, Hallmarks of cancer: the next generation, Cell, 144 (2011) 646-674.

[4] A.D. Bates, A. Maxwell, DNA topology: Topoisomerases keep it simple, Curr. Biol., 7 (1997) R778-R781.

[5] K.D. Corbett, J.M. Berger, Structure, molecular mechanisms, and evolutionary relationships in DNA topoisomerases, Annu. Rev. Biophys. Biomol. Struct., 33 (2004) 95-118.

[6] J.J. Champoux, DNA topoisomerases: Structure, function, and mechanism, Annu. Rev. Biochem., 70 (2001) 369-413.

[7] J.E. Deweese, N. Osheroff, The DNA cleavage reaction of topoisomerase II: wolf in sheep's clothing, Nucleic Acids Res., 37 (2009) 738-748.

[8] A.J. Schoeffler, J.M. Berger, DNA topoisomerases: harnessing and constraining energy to govern chromosome topology, Q. Rev. Biophys., 41 (2008) 41-101.

[9] J.M. Berger, S.J. Gamblin, S.C. Harrison, J.C. Wang, Structure and mechanism of DNA topoisomerase II Nature, 380 (1996) 225-232.

[10] J.M. Berger, J.C. Wang, Recent developments in DNA topoisomerase II structure and mechanism, Curr. Opin. Struct. Biol., 6 (1996) 84-90.

[11] B. Pogorelčnik, A. Perdih, T. Solmajer, Recent developments of DNA poisons - human DNA topoisomerase IIα inhibitors - as anticancer agents, Curr. Pharm. Des., 19 (2013) 2474-2488.

[12] B. Pogorelčnik, A. Perdih, T. Solmajer, Recent advances in the development of catalytic inhibitors of human DNA topoisomerase IIα as novel anticancer agents, Curr. Med. Chem., 20 (2013) 694-709.

[13] E.L. Baldwin, N. Osheroff, Etoposide, topoisomerase II and cancer, Curr. Med. Chem. Anticancer Agents, 5 (2005) 363-372.

[14] G. Minotti, P. Menna, E. Salvatorelli, G. Cairo, L. Gianni, Anthracyclines: Molecular advances and pharmacologic developments in antitumor activity and cardiotoxicity, Pharmacol. Rev., 56 (2004) 185-229.

[15] C. Bailly, Contemporary challenges in the design of topoisomerase II inhibitors for cancer chemotherapy, Chem. Rev., 112 (2012) 3611-3640.

[16] C.A. Felix, Secondary leukemias induced by topoisomerase-targeted drugs, Biochim. Biophys. Acta, 1400 (1998) 233-255.

[17] D.C. Case, T.J. Ervin, M.A. Boyd, L.G. Bove, H.L. Sonneborn, S.D. Paul, Phase-II study of aclarubicin in acute myeloblastic-leukemia, Am. J. Clin. Oncol-Canc., 10 (1987) 523-526.

[18] K. Bojanowski, S. Lelievre, J. Markovits, J. Couprie, A. Jacquemin-Sablon, A.K. Larsen, Suramin is an inhibitor of DNA topoisomerase II in vitro and in Chinese hamster fibrosarcoma cells, Proc. Natl. Acad. Sci. U. S. A., 89 (1992) 3025-3029.

[19] J.M. Fortune, N. Osheroff, Merbarone inhibits the catalytic activity of human topoisomerase II alpha by blocking DNA cleavage, J. Biol. Chem., 273 (1998) 17643-17650.

[20] K. Tanabe, Y. Ikegami, R. Ishida, T. Andoh, Inhibition of topoisomerase II by antitumor agents bis(2,6-dioxopiperazine) derivatives, Cancer Res., 51 (1991) 4903-4908.

[21] S. Chang, T. Hu, T.S. Hsieh, Analysis of a core domain in Drosophila DNA topoisomerase II. Targeting of an antitumor agent ICRF-159, J. Biol. Chem., 273 (1998) 19822-19828.

[22] P. Chene, J. Rudloff, J. Schoepfer, P. Furet, P. Meier, Z. Qian, J.M. Schlaeppi, R. Schmitz, T. Radimerski, Catalytic inhibition of topoisomerase II by a novel rationally designed ATP-competitive purine analogue, BMC Chem. Biol., 9 (2009) 1.

[23] P. Furet, J. Schoepfer, T. Radimerski, P. Chene, Discovery of a new class of catalytic topoisomerase II inhibitors targeting the ATP-binding site by structure based design. Part I, Bioorg. Med. Chem. Lett., 19 (2009) 4014-4017.

[24] L.H. Jensen, H. Liang, R. Shoemaker, M. Grauslund, M. Sehested, B.B. Hasinoff, A three-dimensional quantitative structure-activity relationship study of the inhibition of the ATPase activity and the strand passing catalytic activity of topoisomerase IIalpha by substituted purine analogs, Mol. Pharmacol., 70 (2006) 1503-1513.

[25] L.H. Jensen, A.V. Thougaard, M. Grauslund, B. Sokilde, E.V. Carstensen, H.K. Dvinge, D.A. Scudiero, P.B. Jensen, R.H. Shoemaker, M. Sehested, Substituted purine analogues define a novel structural class of catalytic topoisomerase II inhibitors, Cancer Res., 65 (2005) 7470-7477.

[26] Y. Qin, L. Meng, C. Hu, W. Duan, Z. Zuo, L. Lin, X. Zhang, J. Ding, Gambogic acid inhibits the catalytic activity of human topoisomerase IIalpha by binding to its ATPase domain, Mol. Cancer Ther., 6 (2007) 2429-2440.

[27] B. Pogorelčnik, M. Janežič, I. Sosič, S. Gobec, T. Solmajer, A. Perdih, 4,6-Substituted-1,3,5-triazin-2(1H)-ones as monocyclic catalytic inhibitors of human DNA topoisomerase IIα targeting the ATP binding site, Bioorg. Med. Chem., 23 (2015) 4218-4229.

[28] K. Bergant, M. Janežic, K. Valjavec, I. Sosič, S. Pajk, M. Štampar, B. Žegura, S. Gobec, M. Filipič, A. Perdih, Structure-guided optimization of 4,6-substituted-1,3,5-triazin-2(1H)-ones as catalytic inhibitors of human DNA topoisomerase IIα, Eur. J. Med. Chem., 175 (2019) 330-348.

[29] B. Pogorelčnik, M. Brvar, I. Zajc, M. Filipič, T. Solmajer, A. Perdih, Monocyclic 4-amino-6-(phenylamino)-1,3,5-triazines as inhibitors of human DNA topoisomerase IIα, Bioorg. Med. Chem. Lett., 24 (2014) 5762-5768.

[30] B. Pogorelčnik, M. Brvar, B. Žegura, M. Filipič, T. Solmajer, A. Perdih, Discovery of mono- and disubstituted 1h-pyrazolo[3,4]pyrimidines and 9h-purines as catalytic inhibitors of human DNA topoisomerase IIα, ChemMedChem., 10 (2015) 345-359.

[31] M. Janežič, B. Pogorelčnik, M. Brvar, T. Solmajer, A. Perdih, 3-substituted-1 H -indazoles as catalytic inhibitors of the human DNA topoisomerase IIα, ChemistrySelect, 2 (2017) 480-488.

[32] Ž. Jakopin, J. Ilas, M. Barancokova, M. Brvar, P. Tammela, M. Sollner Dolenc, T. Tomasic, D. Kikelj, Discovery of substituted oxadiazoles as a novel scaffold for DNA gyrase inhibitors, Eur. J. Med. Chem., 130 (2017) 171-184.

[33] G. Jones, P. Willett, R.C. Glen, A.R. Leach, R. Taylor, Development and validation of a genetic algorithm for flexible docking, J. Mol. Biol., 267 (1997) 727-748.

[34] G. Wolber, T. Langer, LigandScout: 3-D pharmacophores derived from protein-bound ligands and their use as virtual screening filters, J. Chem. Inf. Model., 45 (2005) 160-169.

[35] M.A. Avery, Protective Groups in Organic Synthesis, third ed., John Wiley & Sons, New York, 1999.

[36] Ž. Jakopin, R. Roškar, M. Dolenc Sollner, Synthesis of 3,5-disubstituted 1,2,4-oxadiazoles as peptidomimetic building blocks, Tetrahedron Lett., 48 (2007) 1465-1468.

[37] Ž. Jakopin, M. Dolenc Sollner, Recent advances in the synthesis of 1,2,4- and 1,3,4-oxadiazoles, Curr. Org. Chem., 12 (2008) 850-898.

[38] A. Maxwell, N.P. Burton, N. O'Hagan, High-throughput assays for DNA gyrase and other topoisomerases, Nucleic Acids Res., 34 (2006) e104.

[39] W.B. Wu, J.B. Ou, Z.H. Huang, S.B. Chen, T.M. Ou, J.H. Tan, D. Li, L.L. Shen, S.L. Huang, L.Q. Gu, Z.S. Huang, Synthesis and evaluation of mansonone F derivatives as topoisomerase inhibitors, Eur. J. Med. Chem., 46 (2011) 3339-3347.

[40] MOSES - Extensive chemoinformatics platform, www.molecular-networks.com/moses

[41] P. Ertl, B. Rohde, P. Selzer, Fast Calculation of Molecular Polar Surface Area as a Sum of Fragment-Based Contributions and Its Application to the Prediction of Drug Transport Properties, J. Med. Chem., 43 (2000) 3714-3717.

[42] K. Bergant, M. Janežič, A. Perdih, Bioassays and in silico methods in the identification of human DNA topoisomerase IIα inhibitors, Curr. Med. Chem., 25 (2018) 3286-3318.

[43] H. Huang, Q. Chen, X. Ku, L.H. Meng, L.P. Lin, X. Wang, C.H. Zhu, Y. Wang, Z. Chen, M. Li, H.L. Jiang, K.X. Chen, J. Ding, H. Liu, A Series of alpha-Heterocyclic Carboxaldehyde Thiosemicarbazones Inhibit Topoisomerase II alpha Catalytic Activity, J. Med. Chem., 53 (2010) 3048-3064.

[44] A. Volkamer, S. Eid, S. Turk, S. Jaeger, F. Rippmann, S. Fulle, Pocketome of human kinases: prioritizing the ATP binding sites of (yet) untapped protein kinases for drug discovery, J. Chem. Inf. Model., 55 (2015) 538-549.

[45] B. Merget, S. Turk, S. Eid, F. Rippmann, S. Fulle, Profiling Prediction of Kinase Inhibitors: Toward the Virtual Assay, J. Med. Chem., 60 (2017) 474-485.

[46] Ž. Skok, N. Zidar, D. Kikelj, J. Ilaš, Dual Inhibitors of Human DNA Topoisomerase II and Other Cancer-Related Targets, J. Med. Chem., 63 (2019) 884-904.

[47] A. Warshel, R.P. Bora, Perspective: Defining and quantifying the role of dynamics in enzyme catalysis, J. Chem. Phys., 144 (2016) 180901-180901.

[48] S. Dominique, Dynophores: Novel Dynamic Pharmacophores, in, Universität zu Berlin, Lebenswissenschaftliche Fakultät., 2015.

[49] M. Bermudez, C. Rakers, G. Wolber, Structural characteristics of the allosteric binding site represent a key to subtype selective modulators of muscarinic acetylcholine receptors, Mol. Inform., 34 (2015) 526-530.

[50] A. Bock, M. Bermudez, F. Krebs, C. Matera, B. Chirinda, D. Sydow, C. Dallanoce, U. Holzgrabe, M. De Amici, M.J. Lohse, G. Wolber, K. Mohr, Ligand Binding Ensembles Determine Graded Agonist Efficacies at a G Protein-coupled Receptor, J. Biol. Chem., 291 (2016) 16375-16389.

[51] J. Aqvist, J. Marelius, The linear interaction energy method for predicting ligand binding free energies, Comb. Chem. High Throughput Screen., 4 (2001) 613-626.

[52] Y.Y. Sham, Z.T. Chu, A. Warshel, Consistent Calculations of pKa's of Ionizable Residues in Proteins: Semi-microscopic and Microscopic Approaches, J. Phys. Chem. B., 101 (1997) 4458-4472.

[53] M. Repič, M. Purg, R. Vianello, J. Mavri, Examining Electrostatic Preorganization in Monoamine Oxidases A and B by Structural Comparison and pKa Calculations, J. Phys. Chem. B., 118 (2014) 4326-4332.

[54] R.O. Dror, R.M. Dirks, J.P. Grossman, H. Xu, D.E. Shaw, Biomolecular simulation: a computational microscope for molecular biology, Annu Rev Biophys., 41 (2012) 429-452.

[55] G.K. Dasika, S.C. Lin, S. Zhao, P. Sung, A. Tomkinson, E.Y. Lee, DNA damage-induced cell cycle checkpoints and DNA strand break repair in development and tumorigenesis, Oncogene, 18 (1999) 7883-7899.

[56] D.J. Smart, H.D. Halicka, G. Schmuck, F. Traganos, Z. Darzynkiewicz, G.M. Williams, Assessment of DNA double-strand breaks and gammaH2AX induced by the topoisomerase II poisons etoposide and mitoxantrone, Mutat. Res., 641 (2008) 43-47.

[57] O.A. Sedelnikova, E.P. Rogakou, I.G. Panyutin, W.M. Bonner, Quantitative detection of (125)IdU-induced DNA double-strand breaks with gamma-H2AX antibody, Radiat. Res., 158 (2002) 486-492.

[58] E.P. Rogakou, C. Boon, C. Redon, W.M. Bonner, Megabase chromatin domains involved in DNA double-strand breaks in vivo, J. Cell Biol., 146 (1999) 905-916.

[59] H. Wei, A.J. Ruthenburg, S.K. Bechis, G.L. Verdine, Nucleotide-dependent domain movement in the ATPase domain of a human type IIA DNA topoisomerase, J. Biol. Chem., 280 (2005) 37041-37047.

[60] J. Kirchmair, P. Markt, S. Distinto, G. Wolber, T. Langer, Evaluation of the performance of 3D virtual screening protocols: RMSD comparisons, enrichment assessments, and decoy selection - What can we learn from earlier mistakes?, J. Comput. Aided Mol. Des., 22 (2008) 213-228.

[61] B.R. Brooks, R.E. Bruccoleri, B.D. Olafson, D.J. States, S. Swaminathan, M. Karplus, Charmm - a Program for Macromolecular Energy, Minimization, and Dynamics Calculations, J. Comput. Chem., 4 (1983) 187-217.

[62] S. Jo, T. Kim, V.G. Iyer, W. Im, Software news and updates - CHARNIM-GUI: A web-based grraphical user interface for CHARMM, J. Comput. Chem., 29 (2008) 1859-1865.

[63] A.D. MacKerell, D. Bashford, M. Bellott, R.L. Dunbrack, J.D. Evanseck, M.J. Field, S. Fischer, J. Gao, H. Guo, S. Ha, D. Joseph-McCarthy, L. Kuchnir, K. Kuczera, F.T.K. Lau, C. Mattos, S. Michnick, T. Ngo, D.T. Nguyen, B. Prodhom, W.E. Reiher, B. Roux, M. Schlenkrich, J.C. Smith, R. Stote, J. Straub, M. Watanabe, J. Wiorkiewicz-Kuczera, D. Yin, M. Karplus, All-atom empirical potential for molecular modeling and dynamics studies of proteins, J. Phys. Chem. B, 102 (1998) 3586-3616.

[64] A.D. Mackerell, M. Feig, C.L. Brooks, Extending the treatment of backbone energetics in protein force fields: Limitations of gas-phase quantum mechanics in reproducing protein conformational distributions in molecular dynamics simulations, J. Comput. Chem., 25 (2004) 1400-1415.

[65] K. Vanommeslaeghe, E. Hatcher, C. Acharya, S. Kundu, S. Zhong, J. Shim, E. Darian, O. Guvench, P. Lopes, I. Vorobyov, A.D. MacKerell, CHARMM general force field: A force field for drug-like molecules compatible with the charmm all-atom additive biological force fields, J. Comput. Chem., 31 (2010) 671-690.

[66] R.E. Trifonov, A.P. Volovodenko, S.N. Vergizov, N.I. Shirinbekov, V.A. Gindin, A.O. Koren, V.A. Ostrovskii, Basicity of Phenyl- and Methyl-Substituted 1,2,4-Oxadiazoles, Helv. Chim. Acta, 88 (2005) 1790-1797.

[67] W.L. Jorgensen, J. Chandrasekhar, J.D. Madura, R.W. Impey, M.L. Klein, Comparison of simple potential functions for simulating liquid water, J. Chem. Phys., 79 (1983) 926-935.

[68] W. Humphrey, A. Dalke, K. Schulten, VMD: Visual molecular dynamics, J. Mol. Graph. Model., 14 (1996) 33-38.

[69] A.J. Ryan, N.M. Gray, P.N. Lowe, C.W. Chung, Effect of detergent on "promiscuous" inhibitors, J. Med. Chem., 46 (2003) 3448-3451.

[70] GraphPad Software, L. J. C. U., www.graphpad.com

[71] S. Campbell, A. Maxwell, The ATP-operated clamp of human DNA topoisomerase IIalpha: hyperstimulation of ATPase by "piggy-back" binding, J. Mol. Biol., 320 (2002) 171-188.

[72] N.J. de Mol, M.J. Fischer, Surface plasmon resonance: a general introduction, Methods Mol. Biol., 627 (2010) 1-14.

Declaration of interests

☒ The authors declare that they have no known competing financial interests or personal relationships that could have appeared to influence the work reported in this paper.

☐The authors declare the following financial interests/personal relationships which may be considered as potential competing interests:

HIGHLIGHTS

- Structure-guided design and synthesis of 3,5-substituted 1,2,4-oxadiazoles
- Catalytic mode of inhibition of human DNA topoisomerase IIα
- Confirmed binding to the isolated ATPase domain of human topo IIα
- Cytotoxicity against MCF-7 breast cancer cell line
- No induction of double-strand breaks (DSB) of MCF-7 cancer cell line